

1 **Spatial-temporal changes in flow hydraulic characteristics and soil loss**
2 **during gully headcut erosion under controlled conditions**
3

4 Mingming Guo^a, Zhuoxin Chen^b, Wenlong Wang^{b,c,*}, Tianchao Wang^d, Qianhua Shi^b, Hongliang
5 Kang^b, Man Zhao^b, Lanqian Feng^c
6

7 a Key laboratory of Mollisols Agroecology, Northeast Institute of Geography and Agroecology,
8 Chinese Academy of Sciences, Harbin 150081, Heilongjiang, China

9 b State Key Laboratory of Soil Erosion and Dryland Farming on the Loess Plateau, Institute of Water
10 and Soil Conservation, Northwest A&F University, Yangling, Shaanxi 712100, China

11 c Institute of Soil and Water Conservation, Chinese Academy of Sciences and Ministry of Water
12 Resources, Yangling, Shaanxi 712100, China

13 d Ulanyab Grassland Station, Jining, Inner Mongolia 012000, China

14 ***Corresponding author:** Wenlong Wang

15 E-mail addresses: nwafu_wwl@163.com; wllwang@nwsuaf.edu.cn
16

17 Abstract

18 The temporal-spatial changes in flow hydraulics and energy consumption and their associated soil
19 erosion remain unclear during gully headcut retreat. A simulated scouring experiment was conducted
20 on five headcut plots consisting of upstream area (UA), gully headwall (GH) and gully bed (GB) to
21 elucidate the temporal-spatial changes in flow hydraulic, energy consumption, and soil loss during
22 headcut erosion. The flow velocity at the brink of headcut increased as a power function of time,
23 whereas the jet velocity entry to plunge pool and jet shear stress logarithmically or linearly decreased
24 over time. The jet properties were significantly affected by upstream flow discharge. The Reynold
25 number, runoff shear stress, and stream power of UA and GB increased as logarithmic or power
26 functions of time, but the Froude number decreased logarithmically over time. ~~The flow of UA and~~
27 ~~GB was supercritical and subcritical, respectively, and transformed to turbulent with inflow~~
28 ~~discharge increased.~~ The Reynold number, shear stress and stream power decreased by 56.0%, 63.8%
29 and 55.9%, respectively, but the Froude number increased by 7.9% when flow dropped from UA to
30 GB. The accumulated ~~runoff~~ energy consumption of UA, GH and GB positions linearly increased
31 with time, ~~and their proportions of energy consumption are 18.3%, 77.7% and 4.0%, respectively.~~
32 91.12% - 99.90% of total flow energy was consumed during headcut erosion, of which the gully
33 head accounted for 77.7% of total energy dissipation followed by UA (18.3%) and GB (4.0%). The
34 soil loss rate of the “UA-GH-GB” system initially rose and then gradually declined and levelled off.
35 The soil loss of UA and GH decreased logarithmically over time, whereas the GB was mainly
36 characterized by sediment deposition. The proportion of soil loss at UA and GH are 11.5% and
37 88.5%, respectively, of which the proportion of deposited sediment on GB reached 3.8%. The change
38 in soil loss of UA, GH and GB was significantly affected by flow hydraulic and jet properties. The
39 critical energy consumption initiating soil erosion of UA, GH, and GB are 1.62 J s^{-1} , 5.79 J s^{-1} and
40 1.64 J s^{-1} , respectively. These results are helpful to ~~reveal~~ deepen the understanding of gully erosion
41 process and hydrodynamic mechanism ~~and also of gully headcut erosion and built headcut migration~~
42 ~~model.~~ can provide scientific basis for the construction of gully erosion model and the design of
43 gully erosion prevention measures.

44

45 **Keywords:** Gully erosion; Hydraulic property; Headcut retreat; ~~Bank collapse~~Mass failure; ~~Loess~~
46 ~~Plateau~~Energy dissipation

47

48 **1 Introduction**

49 Gully erosion is a typical soil erosion process whereby concentrated runoff from an upstream
50 drainage area recurs in a channel and erodes soil from the area through which runoff passed to
51 considerable depth (Poesen et al., 2003; Zhu, 2012). Gully erosion is recognized as the main
52 sediment source in some hilly and gully-dominated watersheds (Poesen et al., 2003; Valentin et al.,
53 2005; Dotterweich et al., 2012). Poesen et al. (2003) reported that soil loss amount caused by gully
54 erosion accounts for 10% - 94% of total soil loss amount based on the collected data from published
55 articles. Moreover, gully erosion can severely damage to infrastructure, enhance the terrain
56 fragmentation, and cause ecosystem instability, land degradation and food safety (~~Poesen et al., 2003;~~
57 ~~de Vente & Poesen, 2005;~~ ~~Li et al., 2015;~~ Vanmaercke et al, 2016; [Zhang et al., 2018;](#)
58 [Hosseinalizadeh et al., 2019;](#) [Arabameri et al., 2020;](#) [Bogale et al., 2020;](#) [Belayneh et al., 2020;](#) [Wen](#)
59 [et al., 2020](#)).

60 As [the primary process](#) ~~one~~ of the gully erosion ~~processes~~, the gully headcut retreat often
61 significantly influences and determines gully erosion (Oostwoud-Wijdenes et al., 2000;
62 Vandekerckhove et al., 2003; Guo et al., 2019). A headcut is defined as a vertical or near-vertical
63 drop or discontinuity on the bed of a gully occurring where flow is concentrated at a knickpoint
64 (Hanson et al., 2001; Bennett et al., 2000). Many studies have demonstrated that the gully erosion is
65 the result of the combined actions of plunge pool erosion by jet flow, upstream runoff incision,
66 headwall erosion by on-wall flow, mass failure (gully head and wall collapse), (Vanmaercke et al.,
67 2016; Addisie et al., 2017; Guo et al., 2019). Once a headcut is formed in upstream area, the gully
68 will develop rapidly and not stop forward until a critical topographic condition is formed ($S \leq a \cdot A^b$,
69 where S and A is the slope gradient and drainage area upstream gully headcut, respectively) (Kirkby
70 et al., 2003). Moreover, ~~in fact,~~ the ~~erosion processes of~~ different landform units (upstream area, UA;
71 gully head, GH; gully bed, GB) [of gully system exhibited](#) ~~are~~ completely different [erosion processes](#)
72 [and hydrodynamic mechanisms](#) during gully headcut erosion (Zhang et al., 2018; Guo et al., 2019;
73 Shi et al., 2020a). The combination and interaction of erosion processes of the three landform units
74 determined gully headcut erosion process (Vanmaercke et al., 2016). Therefore, clarifying the soil
75 erosion process and characteristics of the three landform units is critical to systematically and clearly

76 reveal the mechanism of gully headcut erosion.

77 Previous studies suggested that gully heacut erosion is affected by various factors including
78 topography, land use change, vegetation, soil properties, and climate (Vanwalleghem et al., 2003;
79 Ionita, 2006; Rodzik et al., 2009; Rieke-Zapp and Nichols, 2011; Torri and Poesen, 2014; Ionita et al.,
80 2015; Vannoppen et al., 2015; Guo et al., 2019, 2020a). In terms of topography, most of studies
81 focused on the threshold relationship ($S \leq a \cdot A^b$) to initiate gully erosion (e.g., Torri and Poesen, 2014).
82 Several experimental studies demonstrated that the upstream slope gradient and headcut height have
83 significant effects on headcut erosion (e.g., Bennett, 1999; Zhang et al., 2018). Land use change is
84 recognized as having the strongest effect on processes related to gully erosion ~~among influencing~~
85 ~~factors~~ (Poesen et al., 2003; Chaplot et al., 2005; Descroix et al., 2008), and also significantly affects
86 the activation of gully headcut erosion (e.g., Torri and Poesen, 2014). In this aspect, the vegetation
87 coverage is a parameter that is often used to clarify its effect on gully erosion (e.g., De Baets et al.,
88 2007; Martínez-Casasnovas et al., 2009), however, in fact, the vegetation effect mainly ~~depended~~
89 ~~depends~~ on the root characteristics and its distribution at gully head (e.g., Vannoppen et al., 2015;
90 Guo et al., 2019). Nevertheless, at present, the most of studies on gully erosion focus on the changes
91 in gully morphology between different periods at a watershed or regional scale (Vanmaercke et al.,
92 2016), which is why the previous studies fail to address the effects of root systems on gully headcut
93 retreat. Guo et al. (2019) concluded that the grass (*Agropyron cristatum*) could reduce soil loss and
94 headcut retreat distance by 45.6–68.5%, 66.9–85.4%, respectively, compared with bare land, and the
95 roots of 0–0.5 mm in diameter showed the ~~–~~greatest controlling influence on headcut erosion. In
96 terms of soil properties, lots of studies have proved the significant effect of soil properties on gully
97 headcut erosion (e.g., Nazari Samani et al., 2010), which ~~was-is~~ mainly related to the change in soil
98 erodibility induced by soil properties including soil texture, soil vertical joints, soluble mineral
99 content, soil lithology, and physicochemical properties (Sanchis et al., 2008; Vanmaercke et al., 2016;
100 Guo et al., 2020a). Rainfall, the main climate factor, is closely related to runoff generation and thus
101 be expected to affect headcut erosion. Many studies have reported that the initiation of gully headcut
102 is correlated with rainfall characteristics (e.g., summation of rainfall from 24-hour rains equal to or
103 greater than 0.5 inches) (Beer and Johnson, 1963; Vandekerckhove et al., 2003; Rieke-Zapp and

104 Nichols, 2011). However, the great difference in the threshold value relating to rainfall factors was
105 found among different areas of the world due to [great-fully different](#) ~~tee-in~~ [erosion environments](#). For
106 example, in the northeast of China, the gully erosion is the result of soil thawing, rainfall runoff and
107 snowmelt runoff (Li et al., 2016b; Xu et al., 2019). Furthermore, at present, the most of studies on
108 gully erosion were conducted to quantify the change in gully erosion (retreat rate, area and volume)
109 at different spatial and temporal scales by using remote sensing interpretation, real-time monitoring
110 and meta-analysis based on literature data (e.g., Vanmaercke et al., 2016). However, the influencing
111 mechanism of these factors on gully headcut erosion is still unclear and need to be revealed in future
112 studies.

113 Evidently, the concentrated flow upstream gully head, mainly depended on the [drainage](#)
114 ~~upstream~~ area [upstream gully heads](#) and rainfall [characteristics](#), is the main and original drive force
115 triggering headcut erosion. The runoff firstly eroded the upstream area and then was parted into two
116 types of flow (on-wall flow and jet flow) at the brinkpoint of gully headcut ([Guo et al., 2021a](#)).
117 Consequently, the on-wall flow persistently eroded the headwall soil, and the jet flow violently
118 impacted gully bed soil and formed a plunge pool (Su et al., 2015; Guo et al., 2019). Subsequently,
119 the two types of flow merged again and eroded gully bed together (Zhang et al., 2018; Shi et al.,
120 2020a). The runoff hydraulic or jet flow properties at different landform units (upstream area, gully
121 head and gully bed) are significantly different, which is an important reason for the difference in
122 erosion process among different landform units. However, the temporal-spatial change in runoff and
123 jet properties during headcut erosion is still unclear and thus needs to be clarified. Furthermore, at
124 present, some experimental studies on headcut erosion of rill, ephemeral gully, gully and bank gully
125 were conducted to investigate the runoff properties, energy consumption, sediment transport process,
126 morphology evolution and empirical model (Bennett and Casalí, 2001; Wells et al., 2009a, 2009b; Su
127 et al., 2014; Xu et al., 2017a; Guo et al., 2019; Shi et al., 2020a). However, relatively few
128 knowledges were obtained to systemically reveal the hydrodynamic mechanism of gully headcut
129 erosion. Therefore, elucidating the temporal-spatial changes in runoff hydraulic and soil loss and
130 hydrodynamic mechanism of UA, GH and GB is of great importance to systematically reveal the
131 hydrodynamics mechanism of gully headcut erosion.

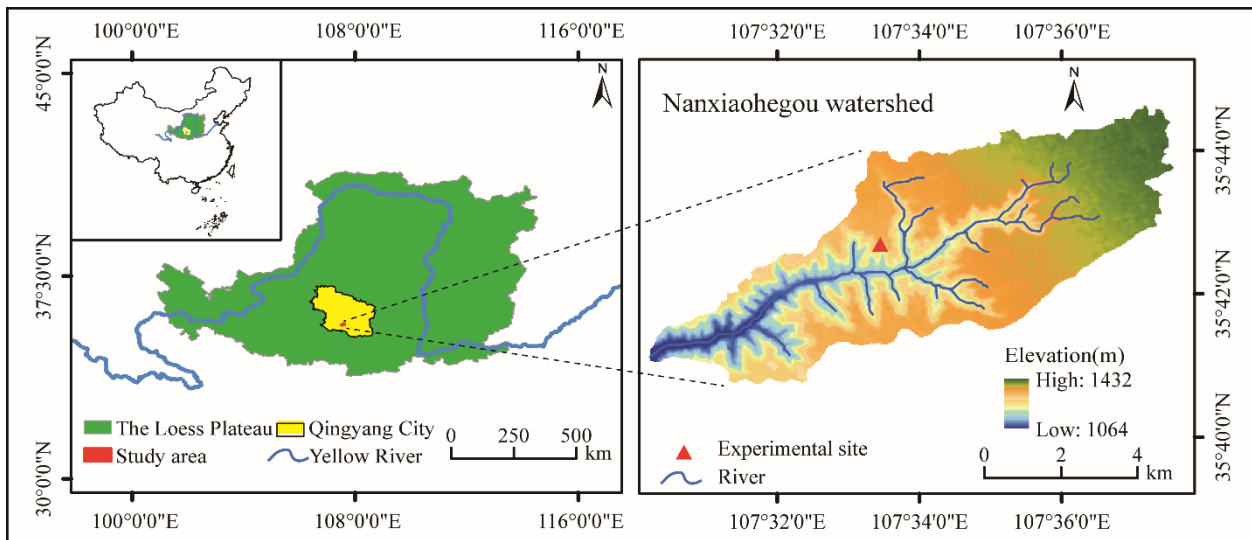
132 Given the above-mentioned issues, a series of simulated gully headcut erosion experiments
133 subjected to inflow scouring are conducted to (1) investigate the temporal-spatial change in [runoff](#)
134 hydraulic [properties](#) and [soil loss jet flow properties](#) during headcut erosion, (2) quantify the [dynamic](#)
135 [change of](#) energy consumption and soil loss [and their spatial](#) distribution ~~of UA, GH and GB~~, and (3)
136 reveal the erosion hydrodynamic mechanism of UA, GH and GB.

137 **2 Materials and Methods**

138 **2.1 Study area**

139 This experiment was carried out at the Xifeng Soil and Water Conservation Experimental
140 Station that is located in the Nanxiaohegou watershed, Qingyang City, Gansu Province, China (~~Fig.~~
141 ~~4~~). The study area belongs to a semi-arid continental climate with a mean annual temperature of
142 9.3 °C. The mean annual precipitation is 546.8 mm (1954 - 2014), of which precipitation from May
143 to September accounts for 76.9% of the total precipitation ([Xia et al., 2017; Guo et al., 2019](#)). The
144 elevation ranges from 1050 to 1423 m (~~Xia et al., 2017; Guo et al., 2019~~). The main landforms
145 include gentle loess-tableland, steep hillslope and gully channel, and their areas account for 57.0%,
146 15.7% and 27.3%, respectively. The loess-tableland is characterized by low slope (1–5°), gentle and
147 flat terrain and fertile soil. The main soil type is loessial soil with silt loam texture. Most of hillslopes
148 have been constructed as slope-terraces. The main gully channel is usually U-shaped and the
149 branch-gully is more actively developed and easily eroded as a V-shaped by runoff from
150 loess-tableland (Xu et al., 2019). The flat loess-tableland can accumulate the 67.4% of total runoff
151 and cause serious gully erosion that can contribute 86.3% of the total soil erosion (Guo et al., 2019).
152 The original plant species have been seriously destroyed. Since the 1970s, the “Three Protection
153 Belts” system, the “Four Eco-Economical Belts” system and the “Grain for Green” project (Zhao,
154 1994; Fu et al., 2011) were implemented to control soil erosion. [The main land use on loess-tableland](#)
155 [position has always been farmland and orchards, while the land use on hillslope is sloping farmland](#)
156 [and orchards before 1999, which have been changed into forested and grassy land due to the “Grain](#)
157 [for Green” project](#). The current mean annual soil erosion rate has been reduced to 4350 ~~t~~[Mg](#) km⁻² y⁻¹
158 in the study watershed (Guo et al., 2019). The ~~previous vegetation plants~~ are ~~primarily~~[mainly](#)
159 artificially planted ~~arbors and herbaceous vegetation and shrubs (Guo et al., 2021b)~~[forests and some](#)

160 native secondary herbaceous communities.



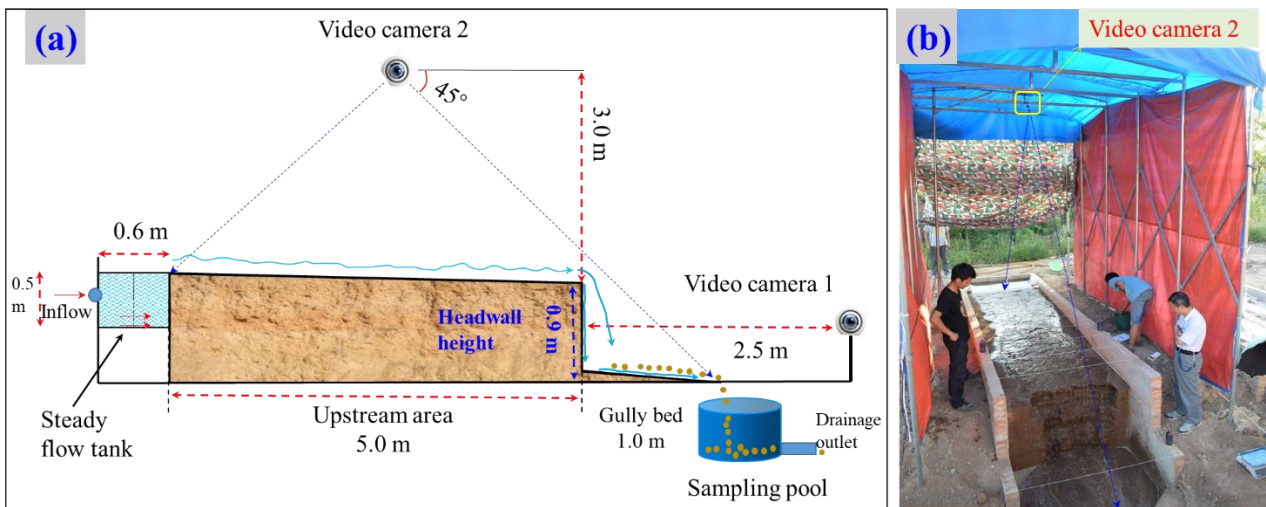
161
162 **Figure 1** The location of the experimental site in Nanxiaohegou watershed, Qingyang City, Loess
163 Plateau, China. Note: The figure production was based on the digital elevation model data (spatial
164 resolution of 30 m) which is available from <http://srtm.esi.cgiar.org> (Reuter et al., 2007).
165

166 2.2 Experimental design

167 2.2.1 Gully head experimental plot construction

168 Five gully head plots for headcut erosion experiments were constructed at the experimental
169 station in April 2018. Fig. 2-1 shows the basic information of the gully head plot consisting of three
170 landform units (upstream area, headwall and gully bed). The plot width and slope gradient of
171 upstream area and gully bed are uniformly designed as 1.5 m and 3°, respectively. The upstream area
172 length, the height of the vertical headwall and the length of the gully bed are 5.0 m long, 0.9 m, and
173 1.0 m, respectively (Fig. 2a1a). The plot boundary was constructed in strict accordance with
174 designed plot dimension using cement and bricks (Fig. 2b1b). After the construction of plot boundary,
175 the soil was sieved through a 2 cm sieve with to remove roots and debris and ensure uniform soil
176 underlying condition. The sieved soil was filled into the plot every 10-cm thick layer according to
177 the investigated soil bulk density of gully heads. The soil surface of each layer was harrowed to
178 increase the cohesion between two soil layers (Guo et al., 2019). In general, the filling upstream area
179 length was 5.5 m that was larger than the precise upstream area length (5.0 m). After establishment
180 of gully head plots, the five plots were carefully managed about four months (August 2018) to allow
181 the soil to return to its nearly natural state. During the four-month conservation process, the naturally

182 growing weeds were weeded out in time. Moreover, a flow-steady tank of 0.6 m, 1.5 m and 0.5 m in
 183 length, width and height was installed at the top of upstream area, and a circular sampling pool of 0.6
 184 m in diameter was set at the bottom of the gully bed to collect runoff and sediment (Fig. 2a1a).
 185 According to the pre-experimental results, the length of upstream area can meet the needs of headcut
 186 migration under designed flow discharge ($3.0 - 7.2 \text{ m}^3 \text{ h}^{-1}$) and gully head height (0.9 m), and the
 187 length of gully bed also can satisfy the development of plunge pool by jet flow and stabilize the flow
 188 of gully bed.



189
 190 **Figure 2-1** Sketch (a) and photo (b) of experimental plot.
 191

192 2.2.2 Inflow discharge design

193 The concentrated runoff generated from upstream area is the main force driving gully headcut
 194 erosion. Jiao et al (1999) concluded that the more serious soil erosion is generally caused by “A”
 195 type rainstorm with the rainfall duration of 25 to 178 mins than other types of rainstorms in the Loess
 196 Plateau. Thus, an extreme case of rainfall duration (180 min) was considered in this study, and the
 197 recurrence period of “A” type rainstorm was designed as 30 years. Previous studies indicated that the
 198 rainstorm distribution on the Loess Plateau showed a non-significant change in past decades (Li et
 199 al., 2010; Sun et al., 2016; Wen et al., 2017). Zhang et al. (1983) proposed a statistical equation (Eq.
 200 (1)) for calculating the average rainfall intensity by analyzing 1710 typical rainstorm events in the
 201 Loess Plateau. Then, the inflow discharge was calculated by Eq. (2) that involves the runoff
 202 coefficient, storm intensity and drainage area upstream gully head and ranged from 3.12 to 9.68 m³
 203 h⁻¹. Before the study, we first conducted some preliminary experiments under some flow discharges,

204 ~~and meanwhile Considering considering~~ the pre-experiment effect, finally, we selected the five
205 inflow discharge levels (3.0, 3.6, 4.8, 6.0, and 7.2 m³ h⁻¹).

$$206 \quad RI = \frac{5.09N^{0.379}}{(t+1.4)^{0.74}} \quad (1)$$

207 where RI is the average rainfall intensity during t minutes, mm min⁻¹; N is the recurrence period
208 of rainstorm, yr; and t is the rainfall duration, min.

$$209 \quad q = \frac{60\alpha \cdot A \cdot RI \cdot w}{W} \quad (2)$$

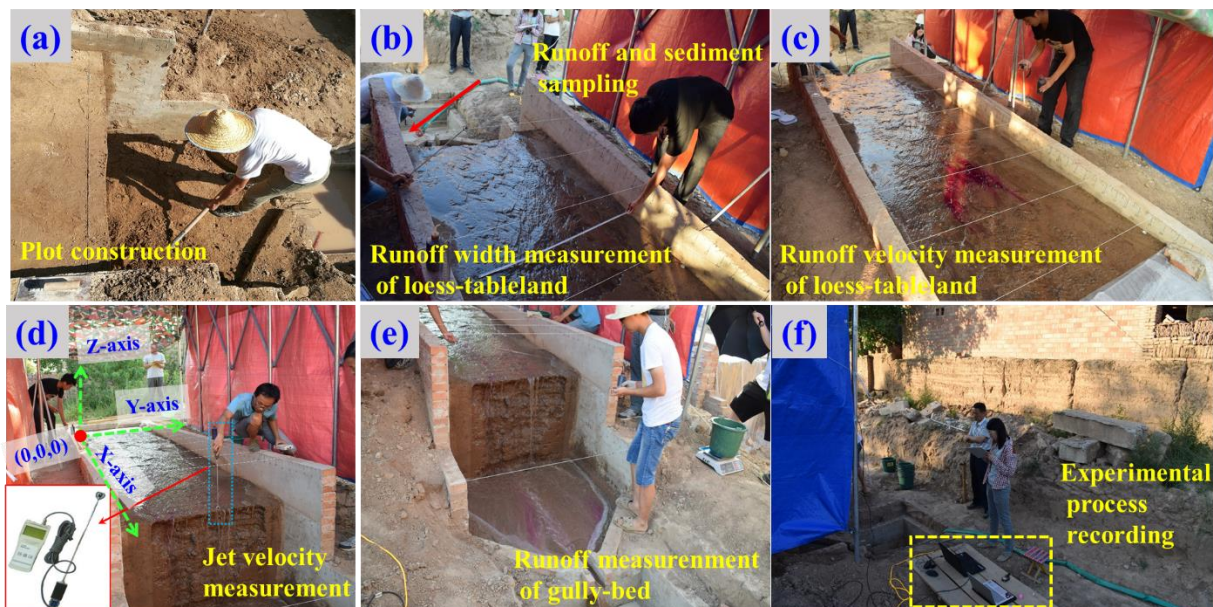
210 where A is the upstream area (km²) and has a wide range of 0.15 - 8.7 km² according to an early
211 investigation of research team (Che, 2012); W is the width of the upstream area, km; w is the plot
212 width, m; and α is the runoff coefficient of bare land and is identified as 0.167 by analyzing the
213 runoff and rainfall data of standard runoff plots (Li et al., 2006).

214 2.3 Experimental procedure

215 The scouring experiment was conducted in August 2018. Before formal experiment, ~~firstly~~, the
216 upstream area length was ~~firstly~~ adjusted to designed length of 5.0 m (Fig. 3a2a). Then, a self-made
217 tent (length × width × height: 6.0 m × 3.0 m × 3.5 m) with waterproof canvas enclosed the plot to
218 resist the effects of natural rainfall and sunshine on experimental progress and photo shooting for 3D
219 reconstruction (Fig. 2b1b). In addition, the experimental process was recorded by two Logitech 930e
220 video cameras with a resolution of 2.0 megapixels. The camera 1 was installed 2.5 m in front of plot
221 headwall (Fig. 2a1a), and the camera 2 was installed 3.0 m above the plot center (Fig. 2a1a).

222 Before the experiment, watering can be used to spray each experimental plot until surface runoff
223 was generated, and then the plot was placed for 24 hours to ensure adequate water infiltration, which
224 can assure that the soil moisture of the five plots was approximately the same. The inlet pipeline was
225 placed in steady flow tank when the inflow discharge was adjusted to designed value. A water
226 thermometer was placed into the steady flow tank to monitor the change in water temperature during
227 ~~experimental process~~. The runoff and sediment samples at the plot outlet were collected at 2-min
228 intervals to represent the temporal change in runoff and sediment of “UA – GH – GB” system, and
229 the sampling time was ~~also~~ recorded using a stopwatch (Fig. 3b2b). The runoff and sediment samples
230 were oven-dried at 105 °C for 24 h and weighed to calculate the soil loss rate of ~~the~~ “UA – GH – GB”
231 system (~~g·s⁻¹~~). Besides, the timing of the collapse events was ~~also~~ recorded during headcut erosion.

232 The upstream area was divided into 4 runoff observation sections, and the runoff width (w), depth (d)
 233 and velocity (V) of each section were measured by a calibrated scale of 1 mm accuracy and color
 234 tracer method (Fig. 3b2b, 3e2c). The runoff velocity (V) before runoff arrived at the brink of headcut
 235 was measured 5 – 8 times by the flow velocity measuring instrument (LS300-A). The instrument was
 236 firstly placed perpendicular to the flow section but does not touch the underlying surface. When the
 237 flow passes through the turbine, the flow velocity can be measured by the rotating velocity of the
 238 turbine with the accuracy of 0.01 m s^{-1} and measuring error of $< 1.5\%$ with the accuracy of 0.01 m s^{-1} ,
 239 and the runoff width at the headcut brinkpoint was measured (Fig. 3d2d). The runoff width and
 240 velocity of gully bed were also measured using the same method with upstream area (Fig. 3e2e).
 241 Above mentioned measurements of runoff characteristics and sediment samples were finished in
 242 2-min intervals. The whole experimental process was recorded by two video cameras and imported
 243 into computers (Fig. 3f2f). In addition to above runoff parameters, the runoff depth (d_b) at the brink
 244 of headcut, the plunge pool depth (D_H) and the vertical distance (h) from brink-point of headcut to
 245 water surface of plunge pool were also measured 3 - 5 times by a steel ruler with 1 mm accuracy
 246 within each 2-min intervals (Fig. 43).



247
 248 **Figure 3-2** Runoff and sediment observation and recording at upstream area, gully head and gully
 249 bed.

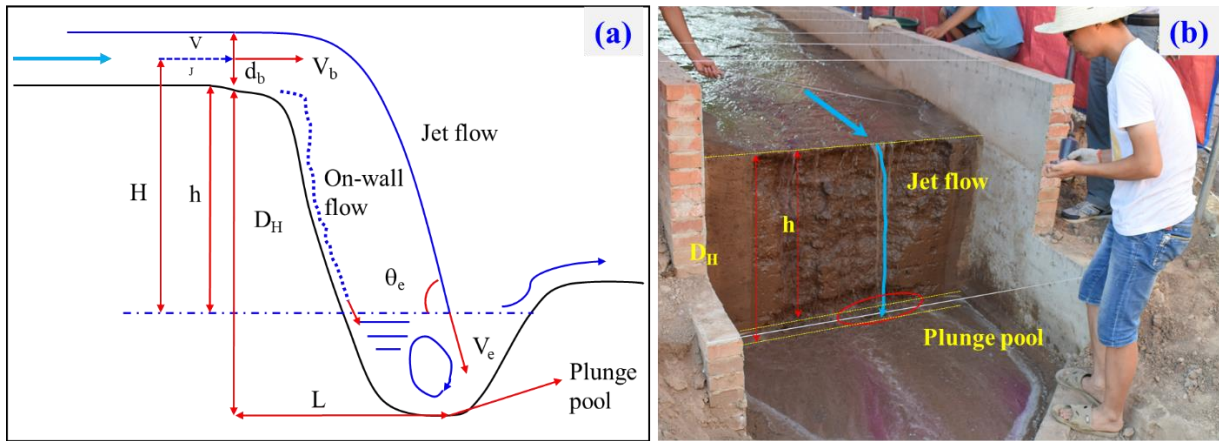


Figure 4-3 Sketch of jet flow at gully headcut and plunge pool at gully bed.

To obtain the temporal-dynamic change in morphology of erosional landformical characteristics during gully headcut erosion, the experimental duration (180 min) was divided into six stage (30 – 60 – 90 – 120 – 150 – 180 min). Photo-based three-dimensional (3D) reconstruction method was employed to obtain the digital elevation model (DEM) data of each plot prior to experiment and after each 30-min test. A total of 14 target points were placed around the plot for identifying the 3D coordinate before the photos were taken. The eroded photographic was recorded by a Nikon D5300 camera with the focal length of 50 mm. The following aspects were required during photos shooting: (1) obvious water on soil surface and direct sunshine should be avoided, (2) a minimum overlap of 60% between subsequent photographs was required, and (3) some complex eroded photographic should be taken in detail. In this study, the upper left corner of the plot was set as the original coordinates (0, 0, 0)-, and the direction of three-dimensional coordinate was determined as shown in Fig. 3d. These collected photos were imported in Agisoft PhotoScan software (Agisoft LLC, Russia, professional version 1.1.6), and then these control points and their coordinates would be identified and entered into the software. The root mean square errors for the altitudes (Z axis) of the target points are 0.0037, 0.0045, 0.0024, 0.0052 and 0.0030 m on average, respectively, for the experiments of five inflow discharges, which can satisfy the study requirement (millimeter level). The DEM could be exported and was used to extract the morphological parameters and soil loss volume of three landform units at six stages (Frankl et al., 2015).

270 2.4 Parameter calculation, data analysis and figure plotting

271 2.4.1 Hydraulic parameters of upstream area and gully bed

272 Five parameters including runoff velocity (V , m s^{-1}), Reynold number (Re), Froude number (Fr),
273 shear stress (τ , Pa) and stream power (ω , W m^{-2}) were used to characterize the changes in hydraulic
274 properties at upstream area and gully bed positions. The ~~five-several~~ parameters except for V are
275 calculated as follows.

$$276 \quad Re = \frac{V \cdot R}{\nu} \quad (1)$$

$$277 \quad Fr = \frac{V}{\sqrt{g \cdot R}} \quad (2)$$

$$278 \quad R = \frac{w \cdot d}{w + 2d}, \nu = \frac{1.775 \times 10^{-6}}{1 + 0.0337T + 0.000221T^2} \quad (3)$$

$$279 \quad \tau = \rho_w \cdot g \cdot R \cdot J \quad (4)$$

$$280 \quad \omega = \tau \cdot V \quad (5)$$

281 where R (m) and ν ($\text{m}^2 \text{s}^{-1}$) are the hydraulic radius and the water kinematic viscosity coefficient,
282 respectively; w (m), d (m) and T ($^{\circ}\text{C}$) are the runoff width, depth and water temperature, respectively;
283 ρ_w (kg m^{-3}) is the water density and J (m m^{-1}) is the hydraulic gradient.

284 2.4.2 Jet properties of gully head

285 Based on the measured runoff velocity (V_J , m s^{-1}) before runoff arrived at the headcut brinkpoint,
286 the runoff depth (d_b , m) at the headcut brinkpoint, the plunge pool depth (D_H , m) and the vertical
287 distance (h , m) (Fig. 43a), the three parameters including the runoff velocity at the headcut
288 brinkpoint (V_b), jet-flow velocity entry to plunge pool (V_e) and jet-flow shear stress (τ_j) were
289 calculated to clarify the change of jet properties (Rouse, 1950; Hager, 1983; Stein et al., 1993;
290 Flores-Cervantes et al., 2006; Zhang et al., 2016). The three parameters were calculated as follows.

$$291 \quad V_b = \begin{cases} \frac{\sqrt[3]{q \cdot g}}{0.715}, Fr < 1 \\ V_J \cdot \frac{Fr^2 + 0.4}{Fr^2}, Fr > 1 \end{cases} \quad \text{--- (5) --- (5) ---}$$

$$292 \quad Fr = \frac{V_J}{\sqrt{g \cdot d_b}} \quad \text{--- (6) --- (6) ---}$$

$$293 \quad V_e = \frac{V_b}{\cos \theta_e}, \theta_e = \arctan \left(\frac{\sqrt{2g \cdot D_H}}{V_b} \right) \quad \text{--- (7) --- (7) ---}$$

$$294 \quad \tau_j = 0.025(V/q)^{0.2} \cdot \rho_w \cdot [2g \cdot (h + d_b/2) + V_b^2] \quad \text{--- (8) --- (8) ---}$$

2.4.3 Energy consumption of upstream area, gully head and gully bed

In this study, energy consumption of three landform units (upstream area, UA; gully head, GH; gully bed, GB) were calculated according to the measured runoff characteristic parameters. The bottom of GB was treated as the zero potential surface to quantify the energy consumption. Therefore, the total runoff energy (E_T , J s⁻¹), the runoff energy at the brink of headcut (E_L , J s⁻¹), the runoff energy when runoff leaves the plunge pool (E_H , J s⁻¹), and the runoff energy at the bottom of gully bed (E_B , J s⁻¹) were calculated as following. [The calculation was consistent with the theory of minimum rate of energy dissipation expressed by Yang \(1971a, 1971b\).](#)

$$E_T = \rho_w g q [(L_l + L_g) \tan \theta + H_h] \quad (9)$$

$$E_L = \rho_w g q [(L_m + L_g) \tan \theta + H_h] + \frac{1}{2} \rho_w q V_J^2 \quad (10)$$

$$E_H = \rho_w g q \left(L_m + L_g - V_b \sqrt{\frac{2h}{g}} \right) \tan \theta + \frac{1}{2} \rho_w q V_P^2 \quad (11)$$

$$E_B = \frac{1}{2} \rho_w q V_B^2 \quad (12)$$

where the L_l (m) and L_g (m) are the projection length of UA and GB, respectively, during gully head migration; L_m (m) is the gully head retreat distance; H_h (m) is the initial gully headcut height. V_P (m s⁻¹) and V_B (m s⁻¹) are the runoff velocity runoff leaving the plunge pool and GB, respectively.

Therefore, the total runoff energy consumption (ΔE_T , J s⁻¹), the runoff energy consumption of UA (ΔE_L , J s⁻¹), the runoff energy consumption of GH (ΔE_H , J s⁻¹) and the runoff energy consumption of GB (ΔE_B , J s⁻¹) could be calculated as follows.

$$\Delta E_T = E_T - E_B \quad (13)$$

$$\Delta E_L = E_T - E_L \quad (14)$$

$$\Delta E_H = E_L - E_H \quad (15)$$

$$\Delta E_B = E_H - E_B \quad (16)$$

2.4.4 Statistical analysis

The curve regression analysis method was employed to determine the quantitative relations between hydraulic characteristics, jet properties, runoff energy consumption and soil erosion rate and inflow discharge. The fitted equations between soil loss rate of three landform units and hydraulic characteristics, jet properties, and energy consumption were also quantified by the curve regression. The soil erosion volume of upstream area, gully head and gully bed were derived from the DEM of

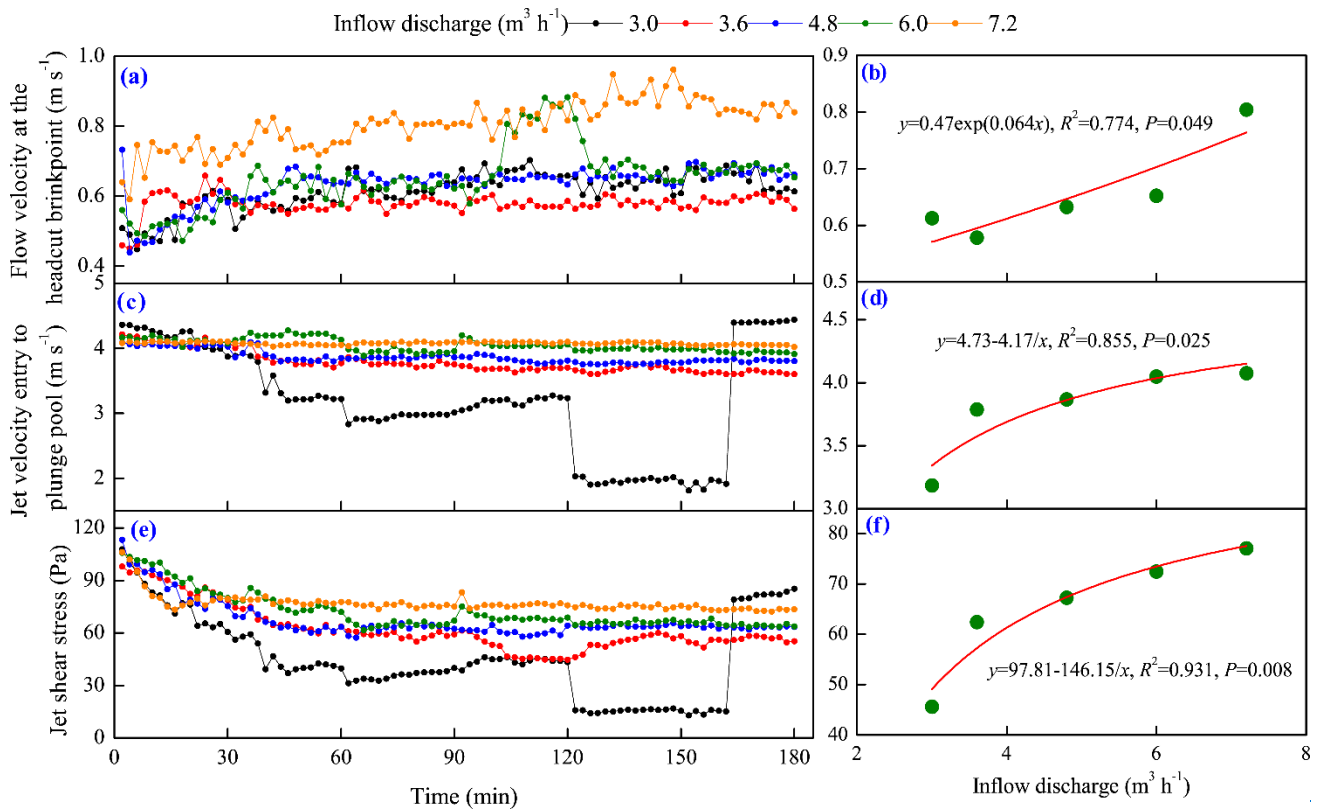
323 different stages through the ArcGIS 10.0 software. The data analyse was executed by using SPSS
324 software (version 6.0) and figure plotting was carried out with Origin 8.5 and PowerPoint 2016
325 software.

326 **3 Results**

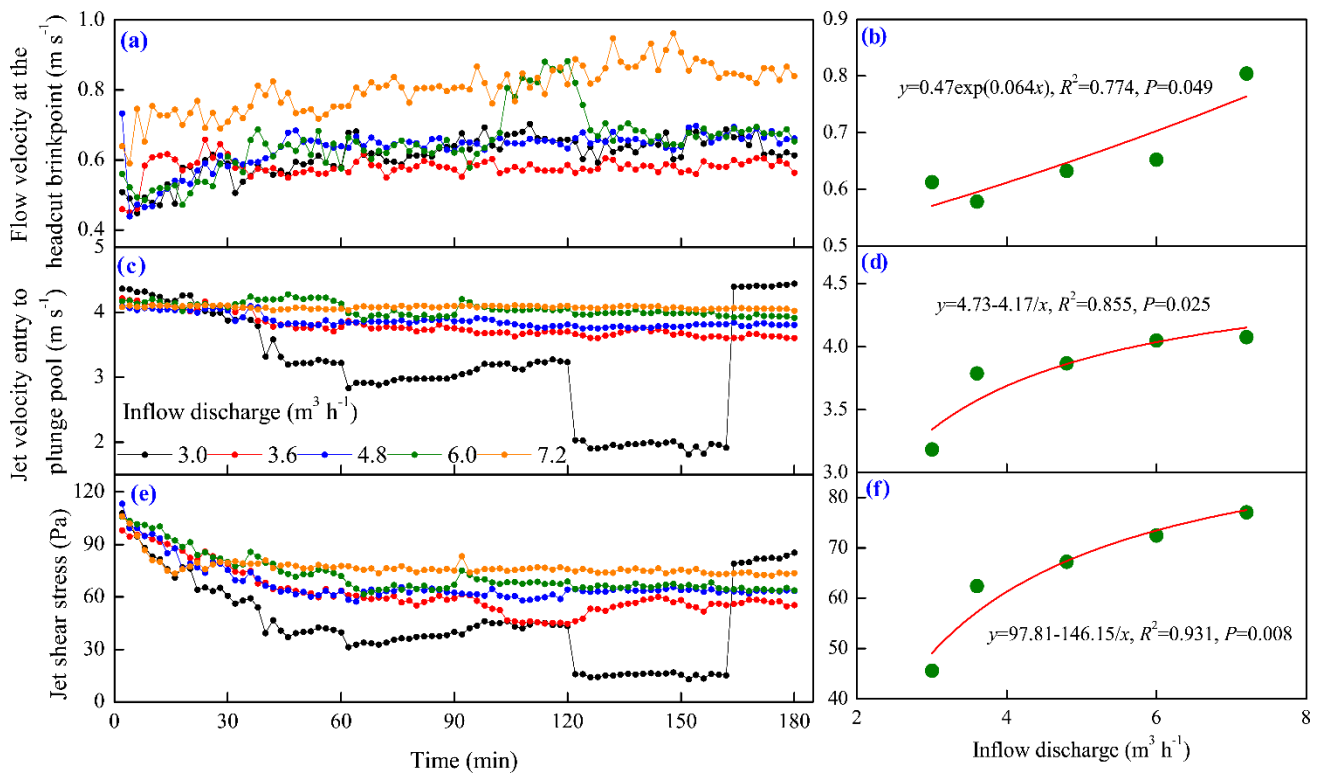
327 **3.1 Spatial-temporal changes in jet properties and runoff hydraulic**

328 **3.1.1 Jet properties of gully head**

329 Fig. 5-4 shows the temporal ~~variation of change in the~~ three jet property parameters of gully
330 head (GH) under different inflow discharge conditions. Overall, the flow velocity at the headcut
331 brinkpoint (V_b) increased obviously in the first 30 min and then showed a gradually stable tendency
332 with some degree of fluctuation (Fig. 5a4a), and the fluctuation degree was enhanced ~~as-by~~ the
333 ~~increased~~ inflow discharge ~~increased~~. For example, the V_b increased sharply from 0.66 to 0.88 m s⁻¹
334 during 100 – 124 min under 6.0 m³ h⁻¹ inflow discharge due to the headwall failure near headcut
335 enhancing the runoff turbulence. Regression analysis revealed the significant power relationships
336 ($V_b = a \cdot t^b$, $R^2 = 0.139 - 0.704$, $P < 0.01$) between V_b and time (t) (Table 1). Furthermore, except for 3.6 m³
337 h⁻¹ condition, the a -value increased with the inflow discharge increased, but the b -value showed a
338 weak variation (0.08 - 0.10), indicating that the flow drainage from gully head ~~could-can~~ improve
339 initial V_b but not change its ~~change~~ trend over time. The mean V_b exhibited a significantly
340 exponential relationship with inflow discharge (Fig. 5b4b, $P < 0.05$). Contrary to the V_b , the jet
341 velocity entry to plunge pool (V_e) and the jet shear stress (τ_j) experienced a gradually decreased trend
342 with time (Fig. 5c4c, 5e4e). Notably, the V_e and τ_j suddenly decreased at 120th min and lasted nearly
343 40 minutes under 3.0 m³ h⁻¹ inflow discharge, which was mainly attributed to the developed second
344 headcut shortening the jet-flow height. The temporal change of V_e could be described by logarithmic
345 functions under 3.0 – 4.8 m³ h⁻¹ inflow discharges, and expressed by linear functions under the other
346 inflow discharges, whereas the decrease of the τ_j with time could be presented by logarithmic
347 functions under all inflow discharge conditions (Table 1). Furthermore, both of mean V_e and τ_j could
348 be expressed by a positive “S” function of inflow discharge (Fig. 5d4d, 5f4f).



349



350

351

352

353

354

355

Figure 5-4 Temporal changes in jet properties of headcut and their relationships with inflow discharge.

Table 1 The relationships between jet properties of gully headcut and time.

Inflow discharge (m ³ h ⁻¹)	$V_b \sim t$	$V_e \sim t$	$\tau_j \sim t$
3.0	$V_b=0.42t^{0.09}, R^2=0.691^{**}$	$V_e=5.28-0.49\lg(t), R^2=0.290^{**}$	$\tau_j=110.86-15.44\lg(t), R^2=0.344^{**}$
3.6	$V_b=0.53t^{0.02}, R^2=0.139^{**}$	$V_e=4.52-0.17\lg(t), R^2=0.859^{**}$	$\tau_j=117.93-13.14\lg(t), R^2=0.823^{**}$
4.8	$V_b=0.46t^{0.08}, R^2=0.544^{**}$	$V_e=4.25-0.09\lg(t), R^2=0.718^{**}$	$\tau_j=109.22-9.93\lg(t), R^2=0.770^{**}$
6.0	$V_b=0.52t^{0.10}, R^2=0.509^{**}$	$V_e=4.17-1.33 \times 10^{-3}t, R^2=0.478^{**}$	$\tau_j=118.73-10.96\lg(t), R^2=0.876^{**}$
7.2	$V_b=0.57t^{0.08}, R^2=0.704^{**}$	$V_e=4.09-1.38 \times 10^{-4}t, R^2=0.111^{**}$	$\tau_j=95.68-4.42\lg(t), R^2=0.619^{**}$

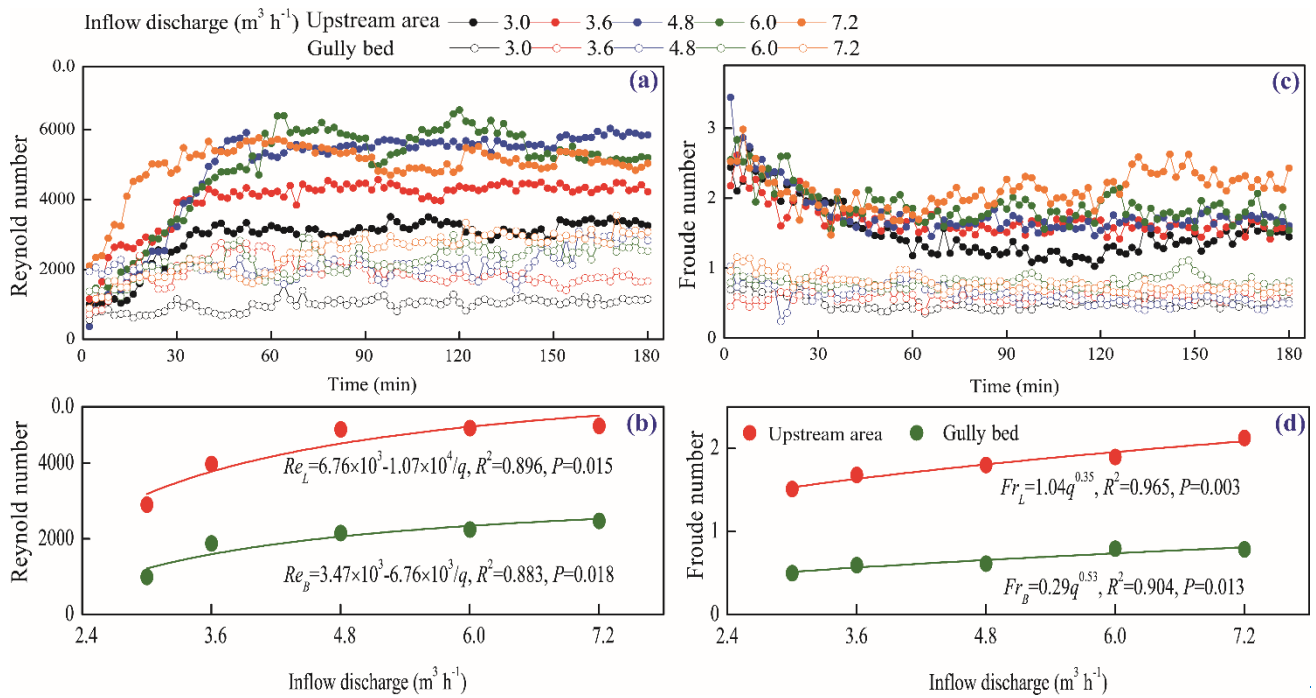
356 Note: V_b , V_e and τ_j are runoff velocity at the headcut brinkpoint, runoff velocity entry to plunge pool and the jet
357 shear stress, respectively. ^{**} refers to the significance of 0.01. The sample number is 90 for the fitted equations.

358 3.1.2 Runoff regime of upstream area and gully bed

359 The temporal changes in runoff Reynold number (Re) and Froude number (Fr) of upstream area
360 (UA) and gully bed (GB) and their relationships with inflow discharge are provided in Fig. 65. The
361 Re of UA and GB showed a similar trend over time, that is, the Re firstly increased in the first 40 min
362 and then gradually stabilized (Fig. 6a5a). In addition, the Re of UA was larger than that of GB at any
363 time under same inflow discharge, indicating that the runoff turbulence became weaker after the
364 runoff of UA passed the gully head. Regression analysis showed that the temporal variation in Re of UA
365 could be described by logarithmic and power functions, but, for the GB, the relationship was mainly
366 dominated by power function (Table 2). On average, the Re of GB was 50.5% - 65.9% less than that
367 of UA, and the Re of UA and GB both increased with the increase of inflow discharge as a power
368 function (Fig. 6b5b). However, as illustrated in Fig. 6e5c, the Fr experienced a completely opposite
369 trend to Re . The Fr of UA decreased in the first 60 min and then gradually stabilized, but the Fr of
370 GB experienced a relatively weak-fluctuating variation over time. For the most of cases, the change
371 in Fr of UA and GB over time could be expressed by logarithmic functions (Table 2). On average,
372 the Fr of UA was 2.39-3.04 times that of GB for same inflow discharge, and the positive power
373 function could describe the relationship between Fr and inflow discharge (Fig. 6d5d).

374 Furthermore, the knowledge of open channel hydraulics is adopted to investigate the difference
375 in runoff regime between UA and GB. The specific definition is: the flow belongs to laminar when
376 Re is less than 500, the flow is turbulent when Re is larger than 2000, and the flow indicates
377 transitional when Re ranges from 500 to 2000; and $Fr = 1$ is the critical value for to distinguish the
378 subcritical and supercritical flow. The six flow regime zones were divided by three boundary lines
379 ($Re = 500$, $Re = 2000$, and $Fr = 1$) according to the logarithmic relationship between the flow

380 velocity and hydraulic radius (Fig. 76) (Xu et al., 2017b; Guo et al., 2020b). ~~As As~~ shown, the runoff
 381 regimes of UA and GB were located in five entirely different zones. The flow of UA was in the
 382 supercritical-transition flow regime in the first 26 min and then gradually transformed to
 383 supercritical-turbulent flow regime under 3.0 – 6.0 m³ h⁻¹ inflow discharge, but the flow ~~at any~~
 384 ~~moment~~ was always in the supercritical-turbulent regime zone under 7.2 m³ h⁻¹ inflow discharge.
 385 Moreover, the higher inflow discharge would enhance the flow turbulent degree. The flow of GB
 386 belonged to subcritical-laminar flow category in the initial 6 min, and then transformed to
 387 subcritical-transition and subcritical-turbulent flow regime when inflow discharge was 3.0 and 3.6
 388 m³ h⁻¹. The flow was in the subcritical-turbulent flow regime in most of experimental duration when
 389 the inflow discharge ~~i~~was 4.8 – 7.2 m³ h⁻¹. The difference in flow regime between UA and GB also
 390 indicated that the presence of gully head can greatly reduce flow turbulence.



391

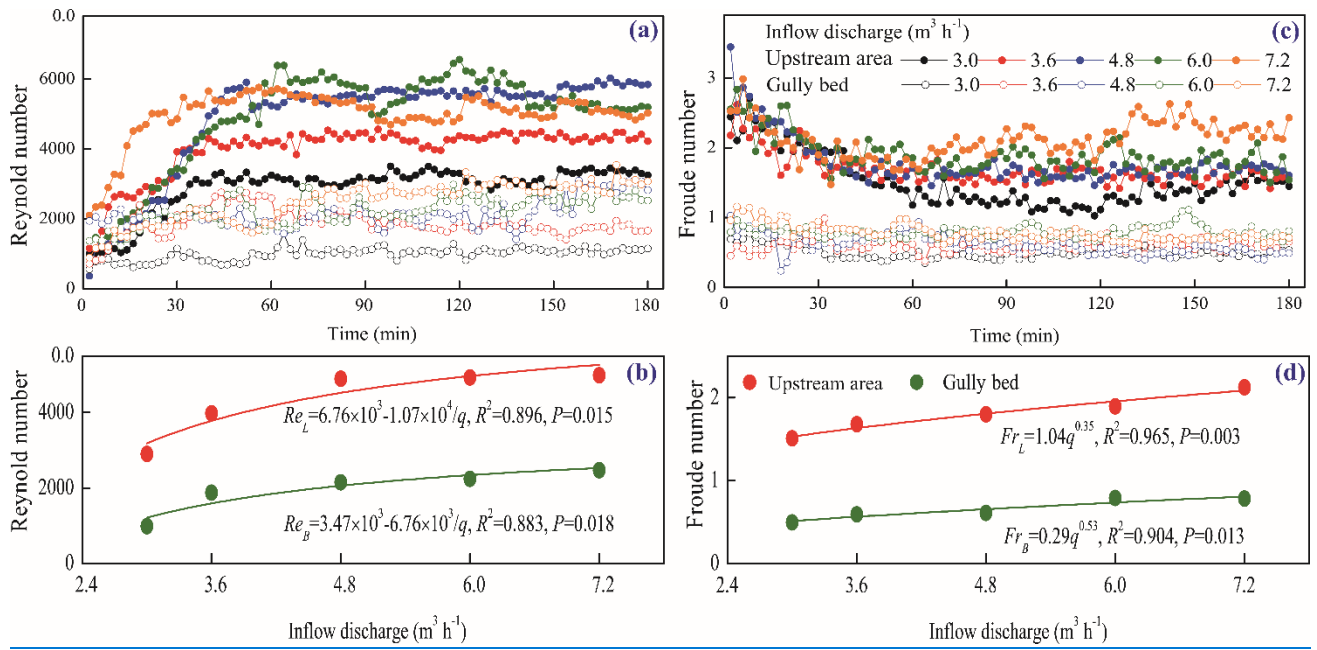


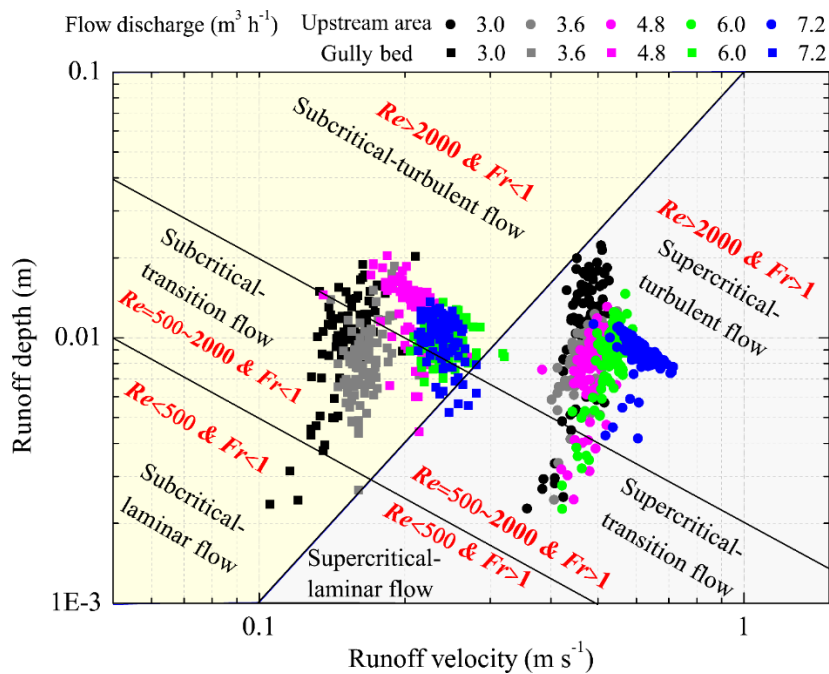
Figure 6-5 Temporal changes in runoff regime of upstream area and gully bed and their relationships with inflow discharge.

392
393
394
395

Table 2 Relationships between runoff hydraulic parameters and time.

Variable	Landfor m unit	Inflow discharge (m ³ h ⁻¹)				
		3.0	3.6	4.8	6.0	7.2
Reynold number	UA	$Re=618.691g(t)$ $+286.69, R^2=0.761^{**}$	$Re=705.931g(t)$ $+1006, R^2=0.815^{**}$	$Re=14331g(t)$ $-1159, R^2=0.849^{**}$	$Re=946.64t^{0.38},$ $R^2=0.794^{**}$	$Re=2760t^{0.14},$ $R^2=0.486^{**}$
	GB	$Re=514.36t^{0.15},$ $R^2=0.504^{**}$	—	$Re=4.31t+1760,$ $R^2=0.334^{**}$	$Re=1.12\times 10^3t^{0.16},$ $R^2=0.566^{**}$	$Re=744.99t^{0.28},$ $R^2=0.872^{**}$
Froude number	UA	$Fr=2.89-0.331g(t),$ $R^2=0.651^{**}$	$Fr=2.46-0.191g(t),$ $R^2=0.651^{**}$	$Fr=3.27-0.351g(t),$ $R^2=0.656^{**}$	$Fr=2.76-0.201g(t),$ $R^2=0.515^{**}$	—
	GB	$Fr=0.72-0.051g(t),$ $R^2=0.326^{**}$	—	$Fr=1.0-0.091g(t),$ $R^2=0.359^{**}$	—	$Fr=1.21-0.101g(t),$ $R^2=0.634^{**}$
Shear stress	UA	$\tau=0.661g(t)+0.55,$ $R^2=0.737^{**}$	$\tau=1.181g(t)+0.78,$ $R^2=0.813^{**}$	$\tau=1.321g(t)-0.62,$ $R^2=0.817^{**}$	$\tau=1.501g(t)-0.63,$ $R^2=0.663^{**}$	$\tau=1.111g(t)+0.99,$ $R^2=0.819^{**}$
	GB	$\tau=2.44t^{0.08},$ $R^2=0.205^{**}$	$\tau=3.88t^{0.05},$ $R^2=0.106^{**}$	$\tau=2.27t^{0.19},$ $R^2=0.664^{**}$	$\tau=3.64t^{0.12},$ $R^2=0.212^{**}$	$\tau=1.99t^{0.27},$ $R^2=0.686^{**}$
Stream power	UA	$\omega=0.341g(t)+0.16,$ $R^2=0.761^{**}$	$\omega=0.381g(t)+0.55,$ $R^2=0.815^{**}$	$\omega=0.781g(t)-0.63,$ $R^2=0.849^{**}$	$\omega=0.691g(t)-0.23,$ $R^2=0.737^{**}$	$\omega=0.271g(t)+1.56,$ $R^2=0.436^{**}$
	GB	$\omega=0.28t^{0.15},$ $R^2=0.504^{**}$	$\omega=0.69t^{0.09},$ $R^2=0.123^{**}$	$\omega=0.50t^{0.19},$ $R^2=0.540^{**}$	$\omega=0.83t^{0.09},$ $R^2=0.338^{**}$	$\omega=0.51t^{0.23},$ $R^2=0.806^{**}$

397 Note: UA and GB refer to upstream area and gully bed. Re , Fr , τ and ω are Reynold number, Froude number, shear
 398 stress, stream power, respectively. ** refers to the significance of 0.01. The sample number is 90 for the fitted
 399 equations.



400

401

Figure 7-6 Runoff regime zones of upstream area and gully bed under different inflow discharge conditions.

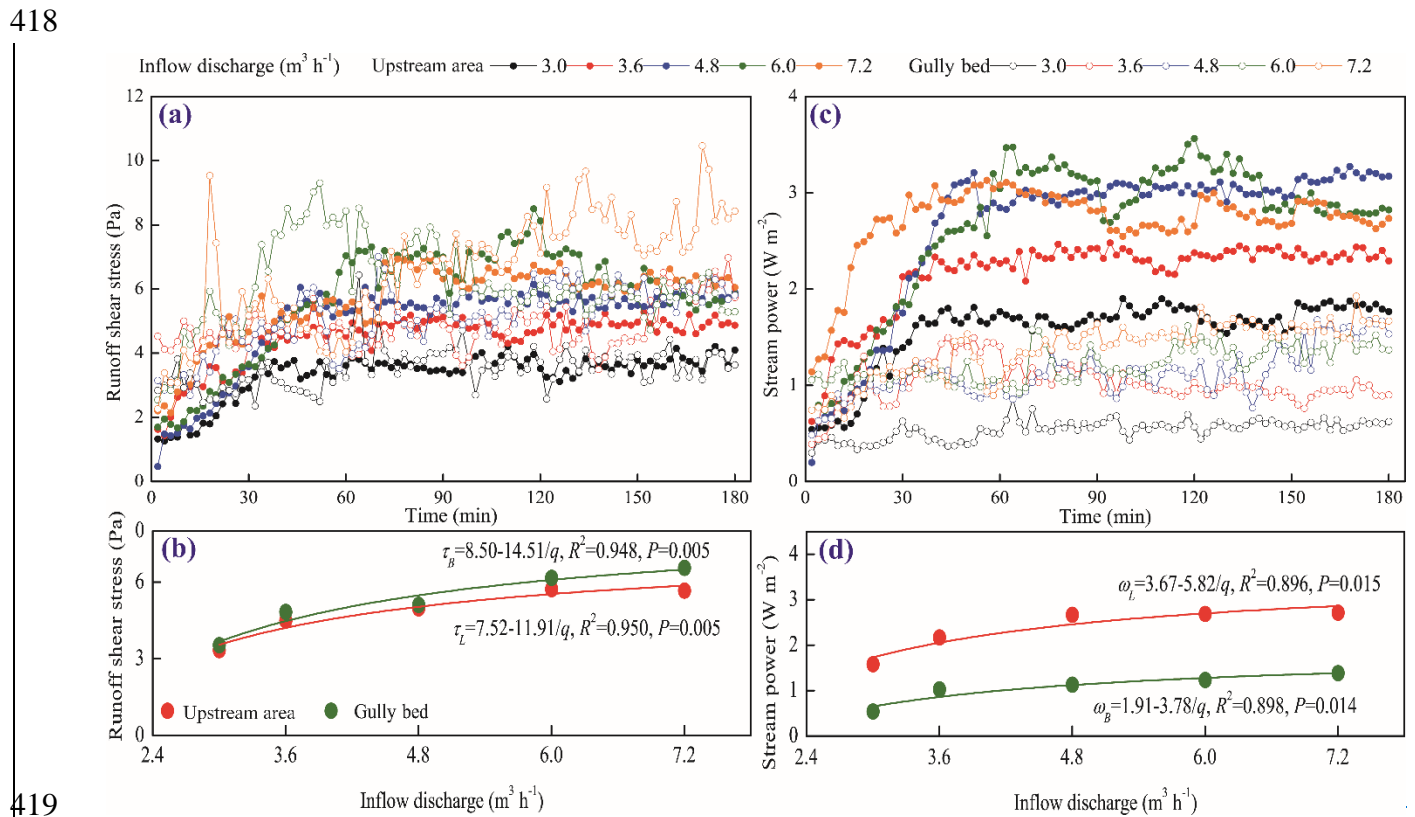
402

3.1.3 Runoff shear stress and stream power of upstream area and gully bed

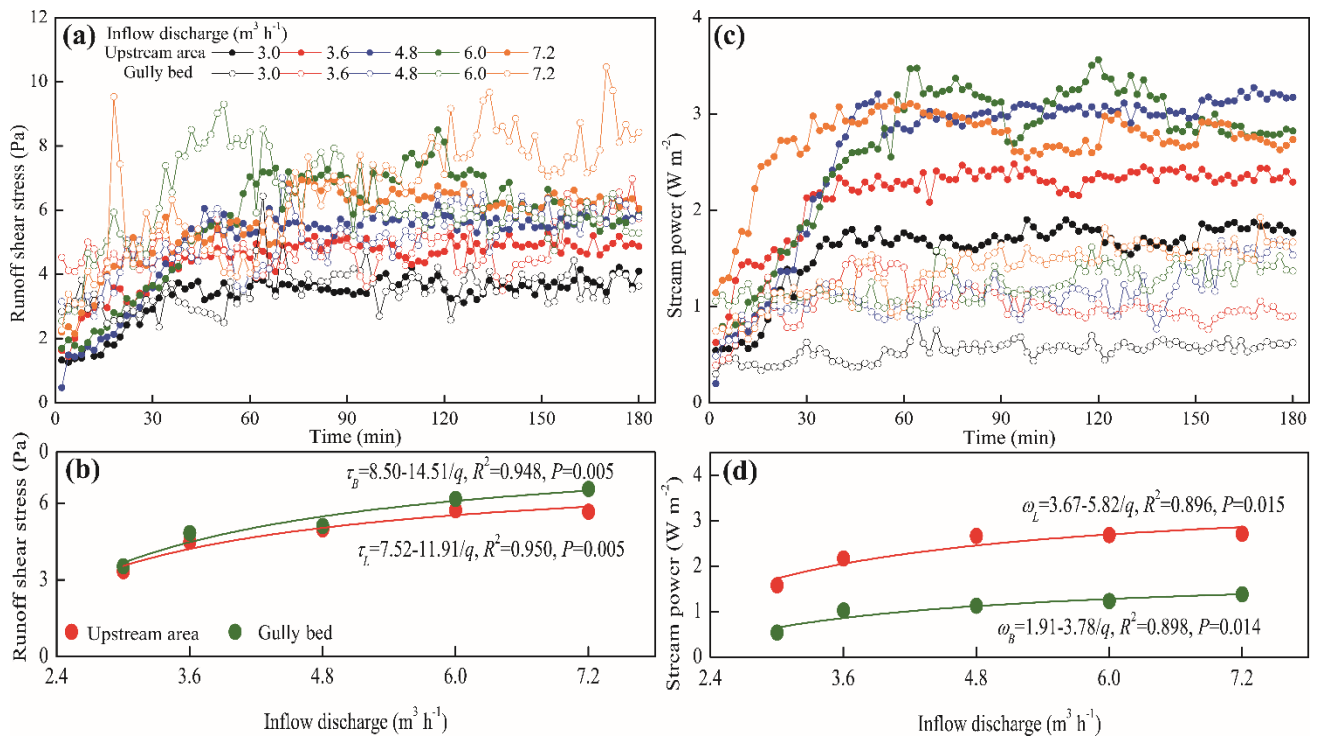
403

Fig. 8-7 shows the temporal changes in runoff shear stress (τ) and stream power (ω) of upstream

404 area (UA) and gully bed (GB) and their relationships with inflow discharge. Overall, the τ of UA and
 405 GB exhibited a gradually increased trend in the first 60 min, and whereafter, a relative steady state
 406 was obtained, but the larger inflow discharge perturbed the steady situation (Fig. 8a7a). Furthermore,
 407 the temporal change in τ of UA could be expressed by logarithmic functions, ~~and~~ but the τ of GB
 408 showed a significant power function with experimental time (Table 2). On average, the τ of GB was
 409 2.8% - 15.7% larger than the UA. The averaged τ of UA and GB increased with inflow discharge as a
 410 power function ($\tau=a-b/q$), and the GB had a faster increased-speed (b -value) than UA (Fig. 8b7b),
 411 signifying that the difference in τ between UA and GB would be widened with the inflow discharge
 412 increased. Similarly, the ω of UA and GB also exhibited a trend of gradual increase and stabilization
 413 over time (Fig. 8e7c). Different from the temporal change in τ , the ω of GB was always less than that
 414 of UA at any time for all-five inflow discharges s-conditions. Likewise, the variation in ω of UA and
 415 GB over time exhibited a significant logarithmic and power function, respectively. On average, the ω
 416 of GB was 49.2% - 65.9% less than UA, and the positive increase in ω of UA and GB with the
 417 inflow discharge could be expressed by a power function (Fig. 8d7d).



419



420
421 **Figure 8-7** Temporal changes in runoff shear stress and stream power of upstream area and gully bed and their
422 relationships with inflow discharge

423 3.2 Spatial-temporal change of energy consumption

424 Fig. 9-8 illustrates the temporal change in accumulated energy consumption of upstream area
425 (UA), gully head (GH) and gully bed (GB). The accumulated energy consumption of the three
426 landform units continued to linearly increase with time ($R^2=0.990-0.999$, $P<0.01$), of which the
427 accumulated energy consumption in GH was always the highest at any time, followed by UA and GB
428 ~~for the experiments of under~~ five inflow discharges. Moreover, the energy consumption rate (the
429 slope-value of fitted equation) in the three landform units is basically constant, indicating the
430 spatial-temporal change in energy consumption maintained a relatively steady state during gully
431 headcut erosion. Moreover, the energy consumption rate of GH was the highest, followed by UA and
432 GB, and the energy consumption rate in the three landform units also increased with the increase of
433 inflow discharge.

434 The variations of total energy consumption of UA, GH and GB and their proportions with
435 inflow discharge are shown in Fig. 109. As illustrated in Fig. 10a9a, both of the total energy
436 consumption of the “UA-GH-GB” system and the three landform units increased with the increase of
437 inflow discharge. When inflow discharge increased from 3.0 to 7.2 $\text{m}^3 \text{h}^{-1}$, the total energy

438 consumption of the system, UA, GH and GB increased by 3.6% - 105.3%, 3.4% - 62.0%, 3.5% -
439 108.2% and 9.0% - 327.5%, respectively. Regression analysis revealed that the energy consumption
440 of the system and the three landform units increased with inflow discharge as an exponential
441 function ($y=a \cdot \exp(b \cdot x)$, $a=1.14 - 55.41$, $b=0.13 - 0.36$, $R^2=0.954 - 0.992$, $P<0.05$). Furthermore, in
442 view of the proportion of energy consumption, the energy consumption of UA accounted for 15.6% -
443 19.8% of total energy consumption, and linearly decreased with inflow discharge increased
444 ($R^2=0.933$, $P<0.05$), whereas the proportion in GB (2.8% - 5.8%) linearly increased with inflow
445 discharge increased ($R^2=0.983$, $P<0.05$). However, the proportion of energy consumption (77.3% -
446 78.6%) in GH showed a weak change with inflow discharge (Fig. ~~40b~~9b), signifying that the most of
447 runoff energy (77.5% on average) was consumed in the gully head position during headcut migration.
448 Furthermore, we found that the total energy consumption (129.89 - 266.60 KJ) under different flow
449 discharge conditions accounted for the 91.12% - 99.90% of total flow energy (Fig. 9c, 9d), which
450 also indicated that only 0.10% - 8.88% of total flow energy remained at the outlet of the
451 “UA-GH-GB” system. These results fully implied that the most of flow energy (>91.12%) upstream
452 from gully heads would be consumed during gully erosion, of which the gully headcut erosion
453 (including plunge pool erosion) is the main process consuming flow energy.

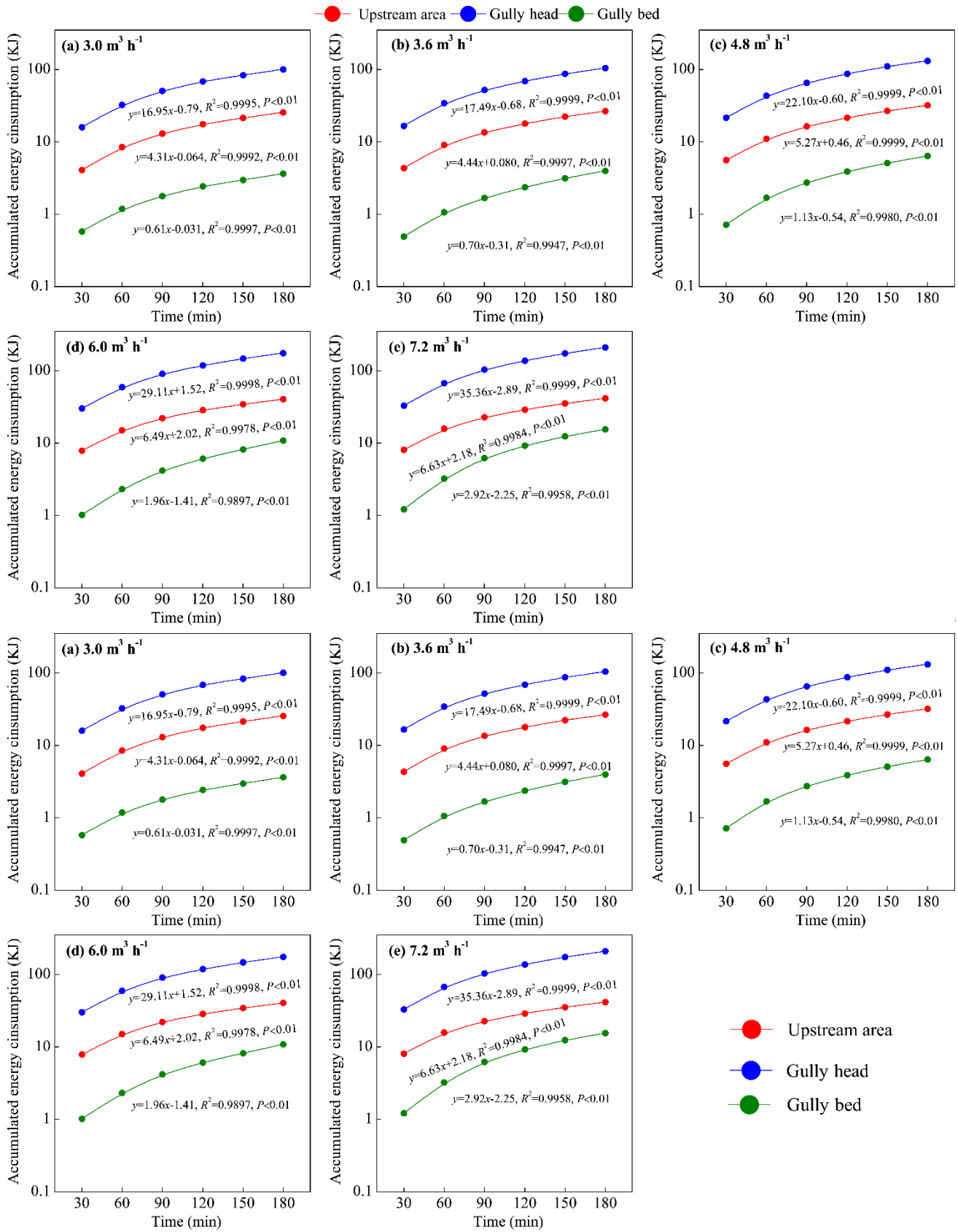
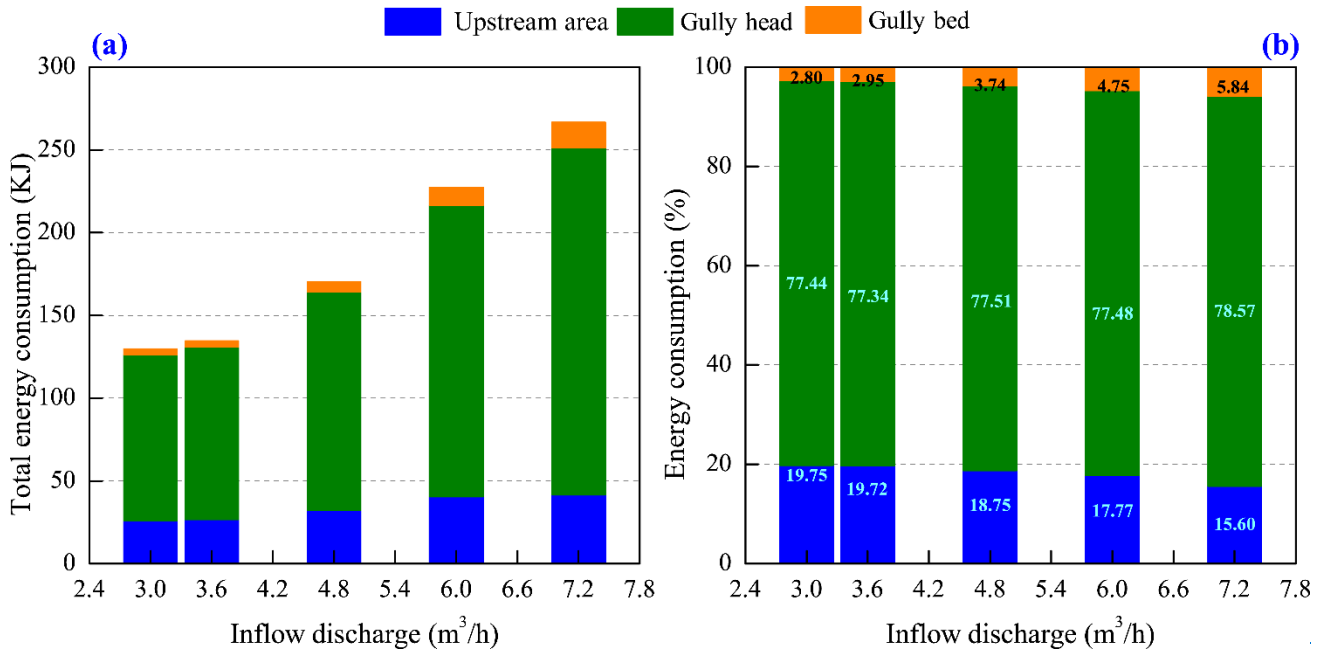
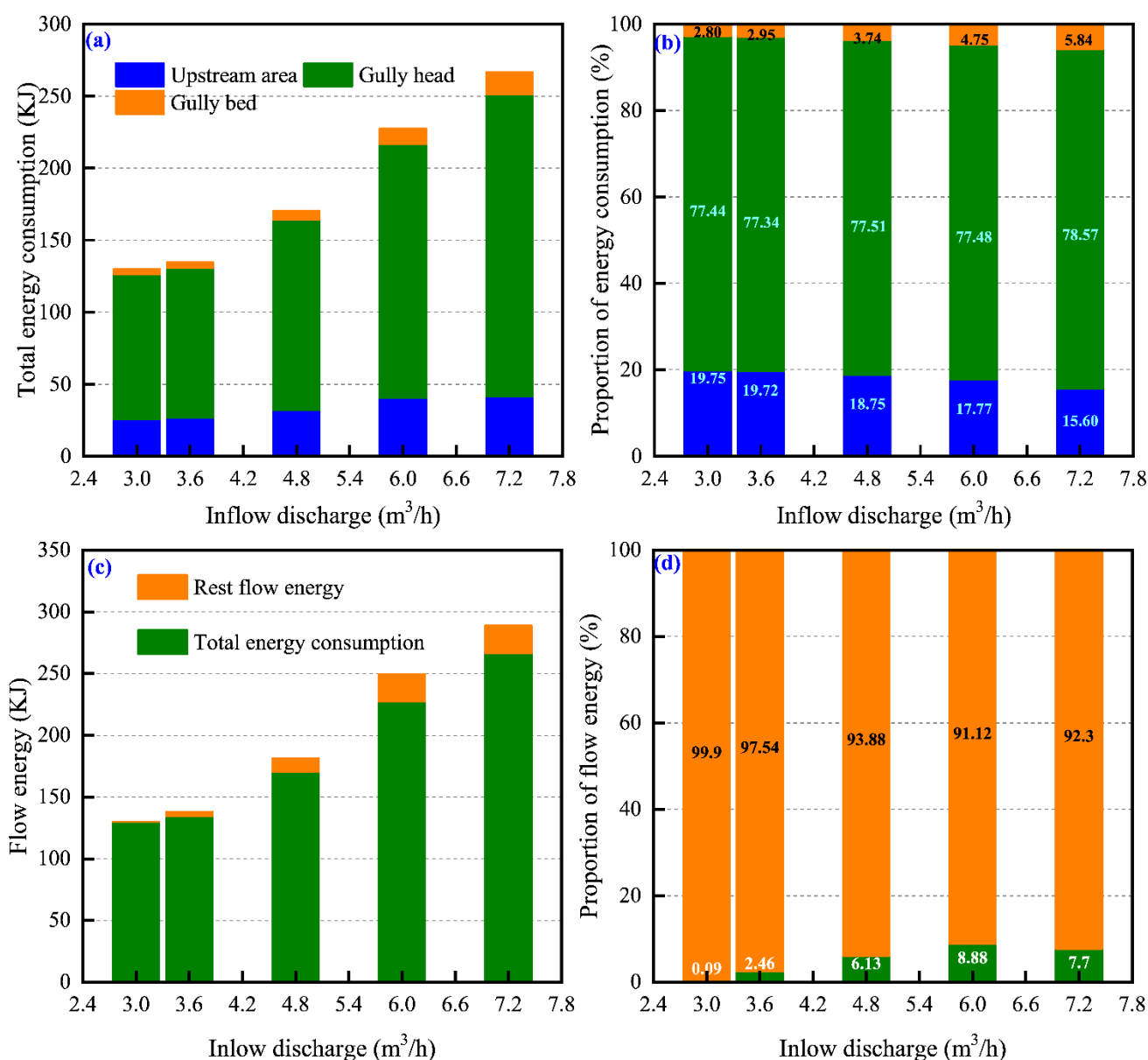


Figure 9-8 Temporal changes in runoff energy consumption of upstream area, gully head and gully bed under different inflow discharge conditions



458



459 **Figure10-Figure 9** The variation in energy consumption of upstream area, gully head and gully bed and their
 460 proportions with inflow discharge
 461

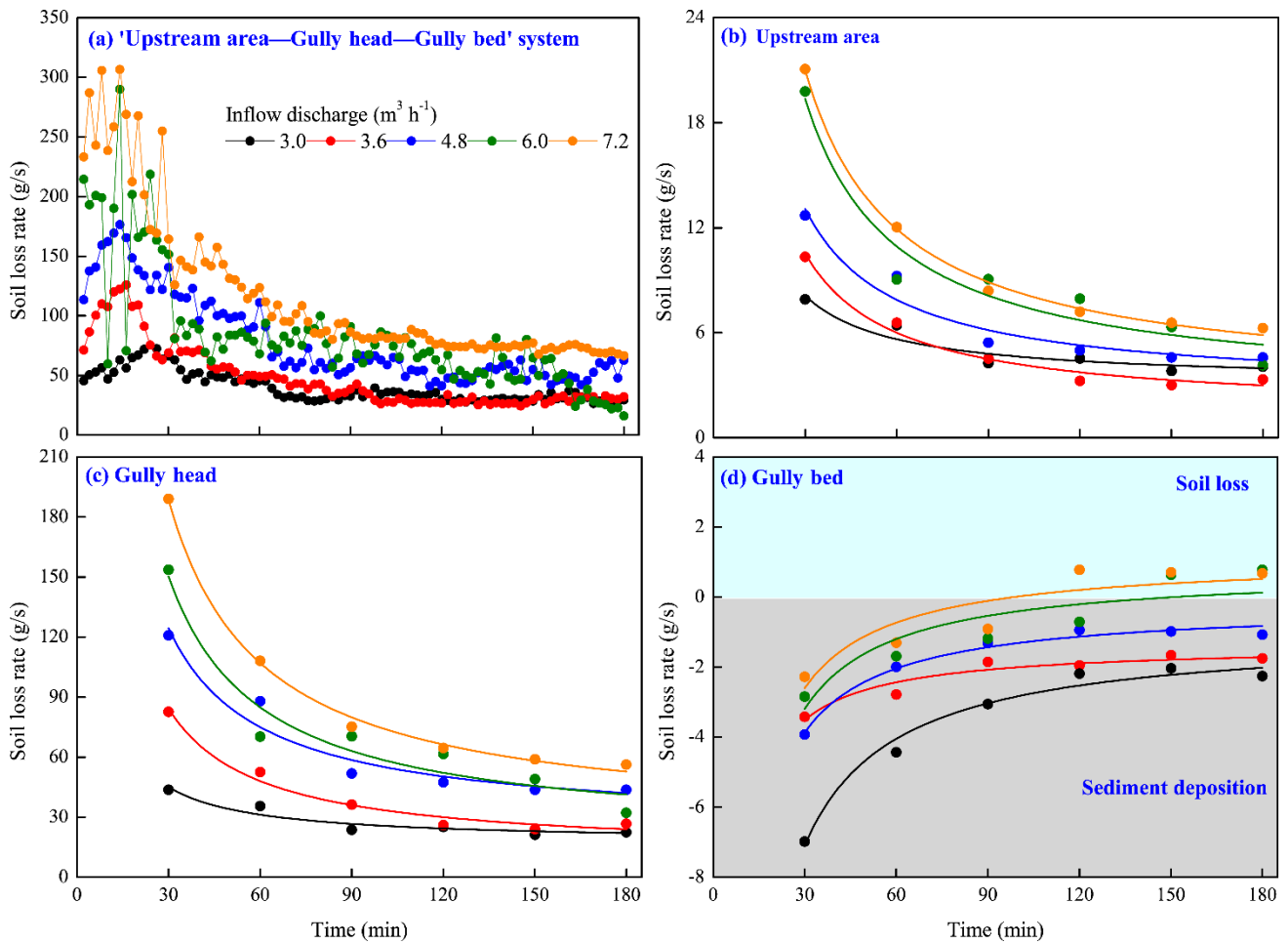
462 3.3 Spatial-temporal change of soil loss

463 3.3.1 Soil loss process

464 Fig. 4a-10a shows that the soil loss rate of the “upstream area (UA)—gully head (GH)—gully
 465 bed (GB)” system rose to a peak in first 20 min, then gradually descend and levelled off. Especially
 466 for the 6.0 and 7.2 m³ h⁻¹, the soil loss rate showed a severe fluctuation trend in the first 30 min. The
 467 peak soil loss rate increased from 75.4 to 306.9 g s⁻¹ with increasing inflow discharge. The soil loss
 468 of UA and GH experienced a similar change process. The soil loss rate was the highest in the early
 469 stage of the experiment, and gradually decreased with time, and became stable after 120 min (Fig.

470 ~~11b10b~~, ~~11e10c~~). Furthermore, the temporal variation in soil loss of UA and GH could be well
471 expressed by logarithmic function ($S_L=a-b\cdot\ln(t)$, $P<0.05$, Table 3), and the a -value (representing
472 initial soil loss rate) and b -value (reflecting the reduction rate of soil loss rate with time) increased
473 with increasing inflow discharge, indicating that larger inflow discharge can improve initial soil loss
474 of UA and GH and also expedite the decrease of soil loss rate.

475 However, the GB presented a completely different soil loss process from UA and GH (Fig.
476 ~~11d10d~~). The GB was always characterized by sediment deposition during the whole experiment for
477 the $3.0 - 4.8 \text{ m}^3 \text{ h}^{-1}$ inflow discharges. The sediment deposition rate gradually decreased with time
478 and presented a significant “S” function over time ($S_B=a/t-b$, $R^2=0.918-0.982$, $P<0.01$, Table 3).
479 When the inflow discharge was larger than $4.8 \text{ m}^3 \text{ h}^{-1}$, the sediment generated from UA and GH was
480 deposited firstly in the GB and then gradually transported, and the temporal change of deposited
481 sediment on GB accorded with logarithmic functions ($R^2=0.936$ and 0.906 , $P<0.01$, Table 3).
482 Furthermore, two critical time points (135 min and 111 min) can be derived from the two fitted
483 logarithmic equations, which distinguished sediment deposition from sediment transport, signifying
484 that the runoff began to transport the deposited sediment ~~deposited~~ on GB after 135 min and 111 min
485 for 6.0 and $7.2 \text{ m}^3 \text{ h}^{-1}$ inflow ~~discharged~~discharges.



486
487
488
489
490

Figure 11-10 Temporal variation in soil loss rate of the “upstream area—gully head—gully bed” system and each landform unit

Table 3 Relationships between soil loss rate of three landform units and time

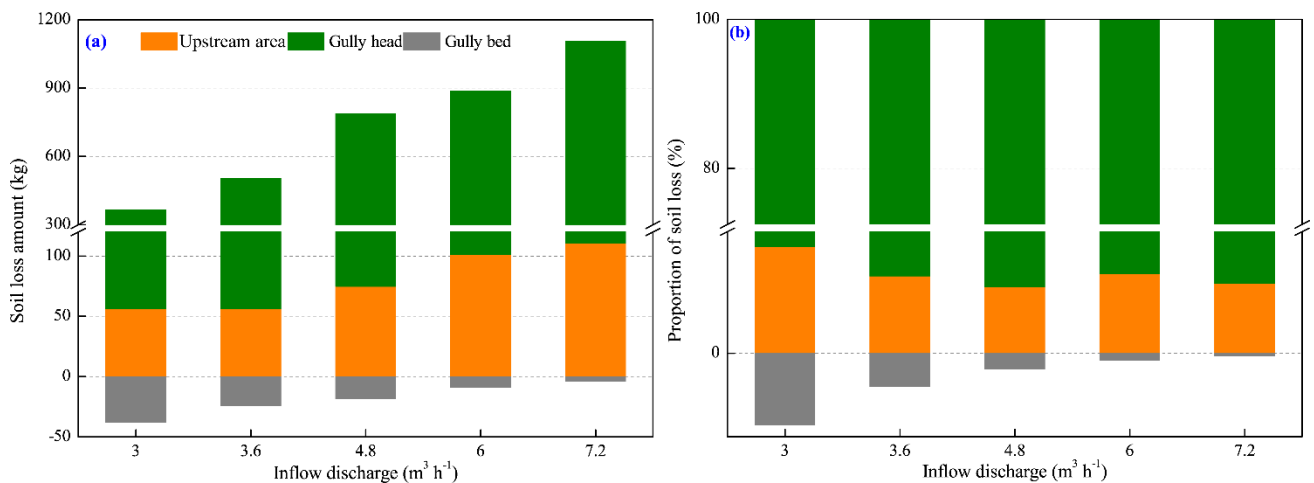
Inflow discharge (m ³ h ⁻¹)	Fitted equations		
	Upstream area	Gully head	Gully bed
3.0	$S_L=15.71-2.34\ln(t)$, $R^2=0.909^{**}$	$S_H=87.12-12.99\ln(t)$, $R^2=0.908^{**}$	$S_B=-182.62/t-1.01$, $R^2=0.980^{**}$
3.6	$S_L=23.97-4.18\ln(t)$, $R^2=0.938^{**}$	$S_H=191.82-33.44\ln(t)$, $R^2=0.939^{**}$	$S_B=-64.46/t-1.36$, $R^2=0.918^{**}$
4.8	$S_L=28.76-4.85\ln(t)$, $R^2=0.930^{**}$	$S_H=273.64-46.17\ln(t)$, $R^2=0.929^{**}$	$S_B=-109.36/t-0.22$, $R^2=0.982^{**}$
6.0	$S_L=44.0-7.69\ln(t)$, $R^2=0.884^*$	$S_H=341.59-59.74\ln(t)$, $R^2=0.885^*$	$S_B=2.03\ln(t)-9.96$, $R^2=0.936^{**}$
7.2	$S_L=47.34-8.25\ln(t)$, $R^2=0.922^{**}$	$S_H=425.24-74.07\ln(t)$, $R^2=0.924^{**}$	$S_B=1.86\ln(t)-8.76$, $R^2=0.906^{**}$

491 Note: S_L , S_H and S_B are the soil loss rate of upstream area, gully head and gully bed, respectively. The sample No. is
492 6 for fitting equation. * and ** indicate the significant level of 0.05 and 0.01.
493

494 3.3.2 Spatial distribution of soil loss

495 The variation in soil loss amount and proportion of the three landform units (UA, GH, GB) with
496 inflow discharge is shown in Fig. 12-11. As illustrated in Fig. 12a-11a, for the experiments of five
497 inflow discharges, the soil loss was dominant in the UA and GH, but the GB was dominated by

498 sediment deposition due to the weaker sediment transport capacity of runoff on GB than sediment
 499 deliverability of UA and GH. Furthermore, the soil loss amount of UA and GH ranged from 55.9 to
 500 110.7 kg and from 310.0 to 994.8 kg, respectively, and increased linearly with increasing inflow
 501 discharge ($R^2=0.966$ and 0.969 , $P<0.05$). The sediment deposition amount of GB ranged from 4.2 to
 502 37.7 kg, and decreased with inflow discharge as a logarithmic function ($R^2=0.961$, $P<0.05$). In terms
 503 of proportion of soil loss (Fig. 12b11b), the proportion of UA and GH reached the maximum (15.3%)
 504 and minimum (84.7%), respectively under $3.0 \text{ m}^3 \text{ h}^{-1}$ inflow discharge, whereas, the proportion
 505 exhibited a little change (UA: 9.5% - 11.4%; GH: 88.6% - 90.5%) when the inflow discharge is 7.2
 506 $\text{m}^3 \text{ h}^{-1}$. Remarkably, the proportion of deposited sediment amount on GB to total soil loss amount
 507 ranged from 0.4% to 10.3%, and decreased exponentially with inflow discharge ($R^2=0.992$,
 508 $P<0.001$).



509
 510 **Figure 12-11** Variation in soil loss amount and proportion of upstream area, gully head and gully bed with inflow
 511 discharge
 512

513 3.4 Spatial change in hydrodynamic mechanism of soil loss

514 3.4.1 Relationships between soil loss and hydraulic parameters

515 Fig. 13-12 indicates the significant difference in the relationships between soil loss rate and
 516 hydraulic parameters among the three landform units (Fig. 13-12). For the upstream area (UA), the
 517 soil loss rate could be described as a series of exponential functions of runoff velocity, Reynold
 518 number, Froude number, runoff shear stress and stream power, of which the runoff shear stress and
 519 stream power showed had a closer correlation with soil loss (Fig. 13a-12a - 13e12e, $R^2=0.830$ –

520 0.945). Furthermore, the increased speed of soil loss rate obviously increased with the increasing
521 hydraulic parameters (except for runoff velocity), indicating that soil loss of UA showed a stronger
522 sensitive response to increasing hydraulic properties. However, the soil loss rate of gully bed (GB)
523 linearly increased with the above-mentioned five parameters (Fig. ~~13f-12f~~ – ~~13j12j~~, $R^2=0.918$ –
524 0.994), which suggested that the decreased rate of sediment deposition of GB is basically constant
525 with the increasing hydraulic properties. Further analysis showed that ~~the there areis~~ critical runoff
526 velocity, Reynold number, Froude number, runoff shear stress and stream power for triggering the
527 transformation of sediment deposition to soil erosion on GB, and the critical values are 0.26 m s⁻¹,
528 2845, 0.85, 6.94 Pa and 0.40 W m⁻², respectively. For the gully head (GH) position, the soil loss was
529 significantly affected by jet velocity entry to plunge pool and jet shear stress (Fig. ~~13l-12l~~ and
530 ~~13m12m~~, $R^2=0.862$ and 0.939), while the relationship between soil loss and flow velocity at the
531 headcut brink-point was not significant (Fig. ~~13k12k~~, $P=0.065$).

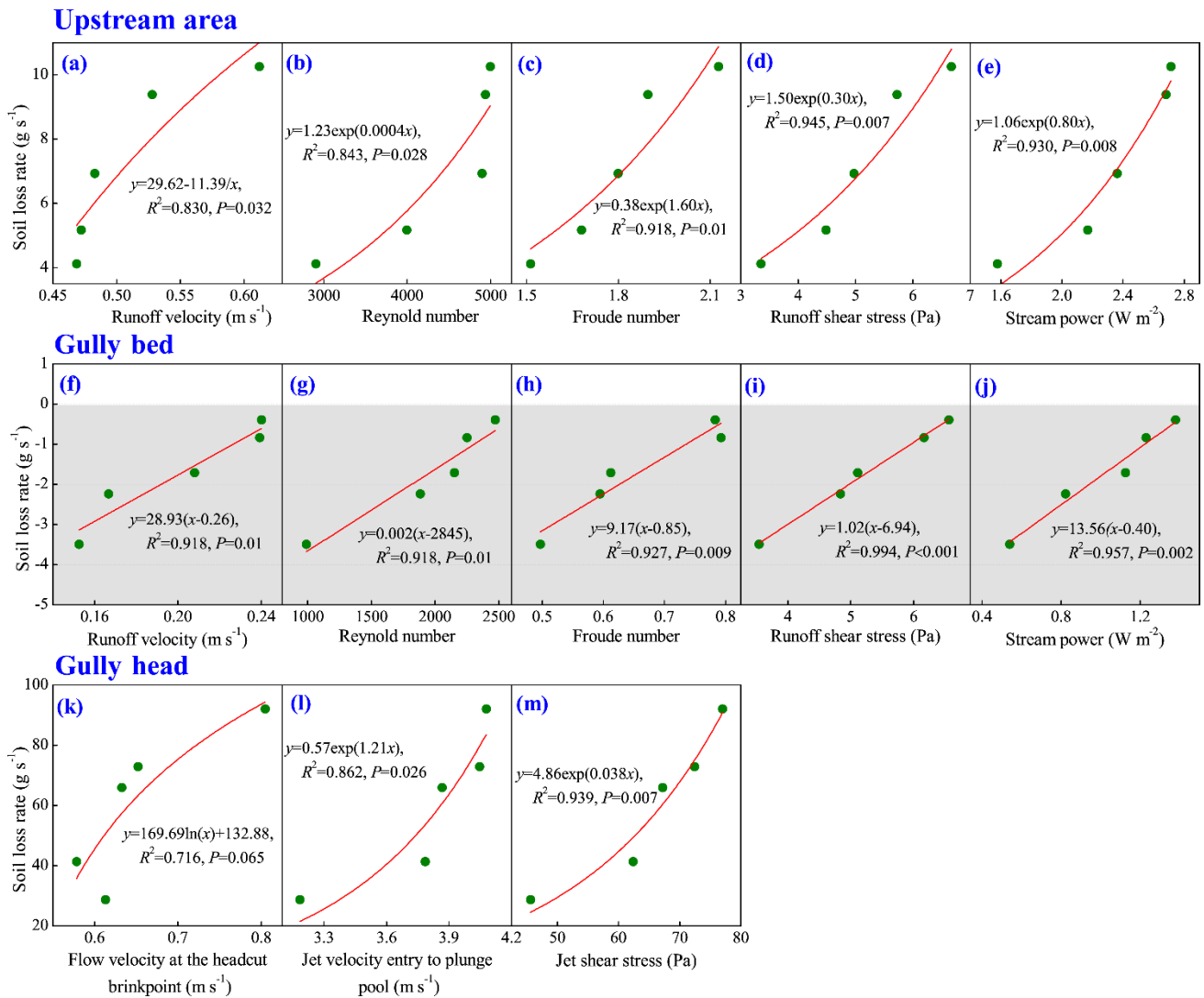


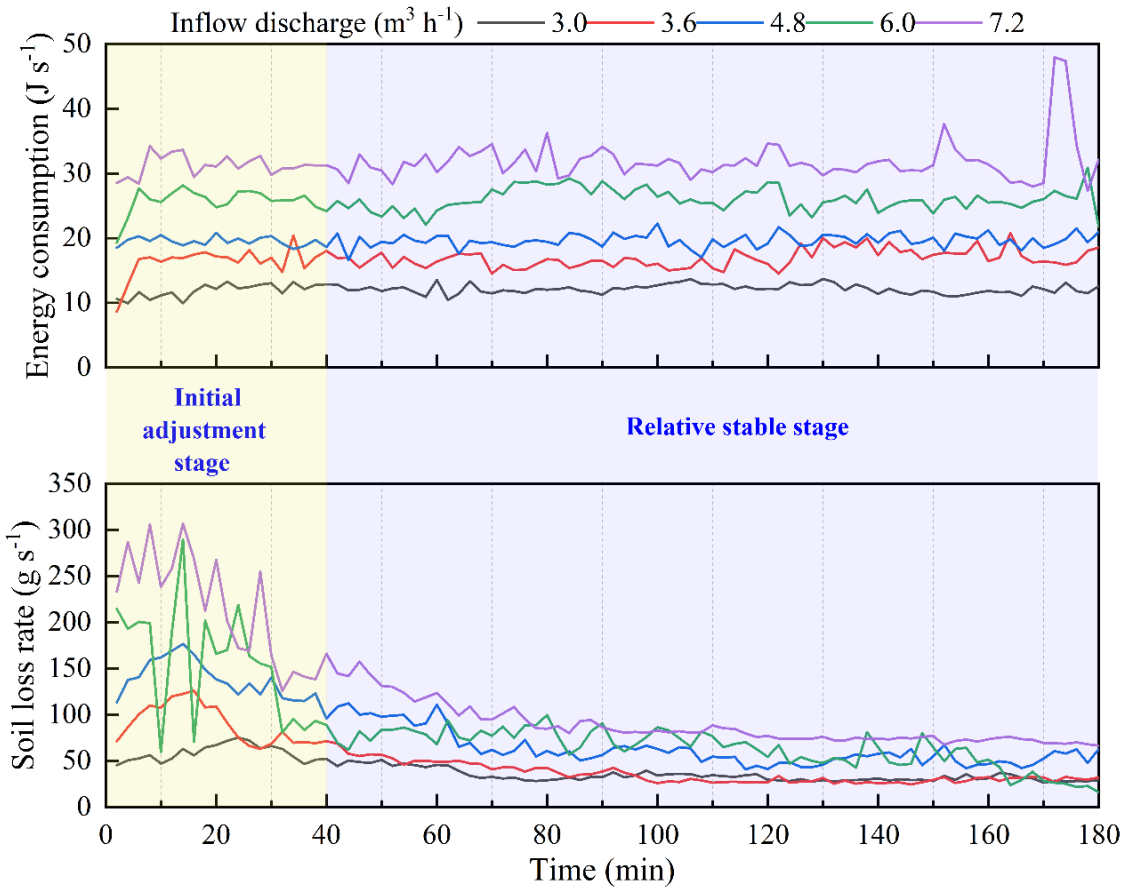
Figure 13-12 Relationships between soil loss rate of three landform units and hydraulic and jet properties

3.4.2 Response of soil loss to energy consumption

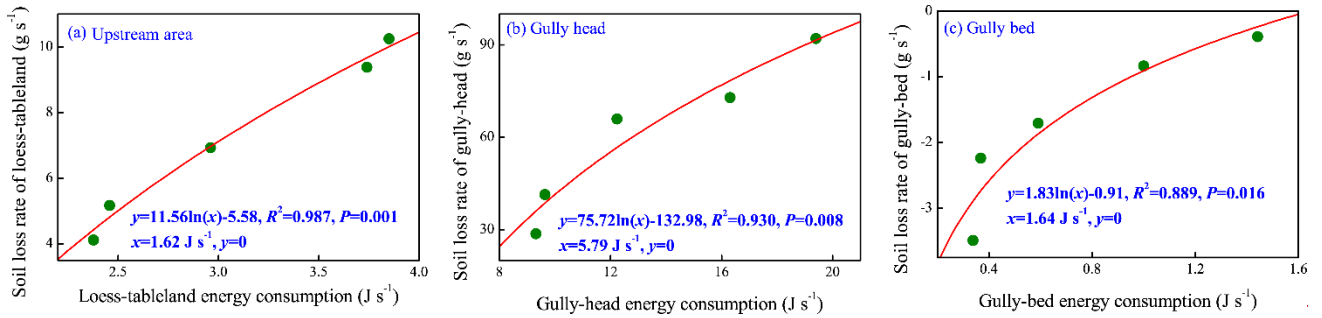
The synchronous change of soil loss of “UA-GH-GB” system and total energy consumption can be divided into two stages (Fig. 13). In the initial adjustment stage (0-40 min), the topsoil layer of UA had the relative higher erodibility and was the main resource of soil loss, which caused the relative lower flow velocity at the brinkpoint of gully head. Therefore, the most of flow discharge was transformed as on-wall flow, so the most of flow energy consumed at the headwall. So, in this stage, UA and gully headwall are the main positions of soil loss, and the most of flow energy was also consumed in the two positions. With the gradual adjustment of upstream area morphology, the gully erosion process entered into the relative stable stage (40-180 min). In this stage, the flow velocity at headcut obviously increased and showed a slight change (Fig. 4a), and thus the headwall

545 erosion and plunge pool erosion also experienced a relative stable process. As a result, the soil loss
546 and flow energy consumption exhibited a similar change process. Occasionally, the occurrence of
547 several gully head and bank collapse events altered the synchronous change process of soil loss and
548 energy consumption.

549 As illustrated in Fig. 14, on average, the soil loss rate of the “UA-GH-GB” system and the three
550 individual landform units was positively and significantly related to the energy consumption
551 ($P < 0.05$), and a logarithmic function was found to fit the relationship between soil loss rate and
552 energy consumption best ($R^2 = 0.889 - 0.987$). The critical energy consumption initiating the system
553 is 7.53 J s^{-1} (Fig. 14a). Furthermore, there is critical energy consumption to initiate soil erosion of the
554 upstream area (UA) and gully head (GH) based on the fitted logarithmic functions (Fig. 14ab, 14cb).
555 The critical energy consumption for GH (5.79 J s^{-1}) is 2.57 times greater than that (1.62 J s^{-1}) of the
556 UA. Similarly, for the gully bed (Fig. 14de), the minimum energy consumption (1.64 J s^{-1}) is needed
557 to trigger the transformation of sediment deposition to soil loss. We found that the sum of critical
558 energy consumption initiating three landform units (9.05 J s^{-1}) was larger than the critical value
559 initiating the system, which was mainly attributed to the mass failure of gully head and bank
560 inputting the additional potential energy into the flow.



561
562 Figure 13 Synchronous change of soil loss rate of “upstream area-gully head-gully bed” system
563 and total energy dissipation during headcut erosion



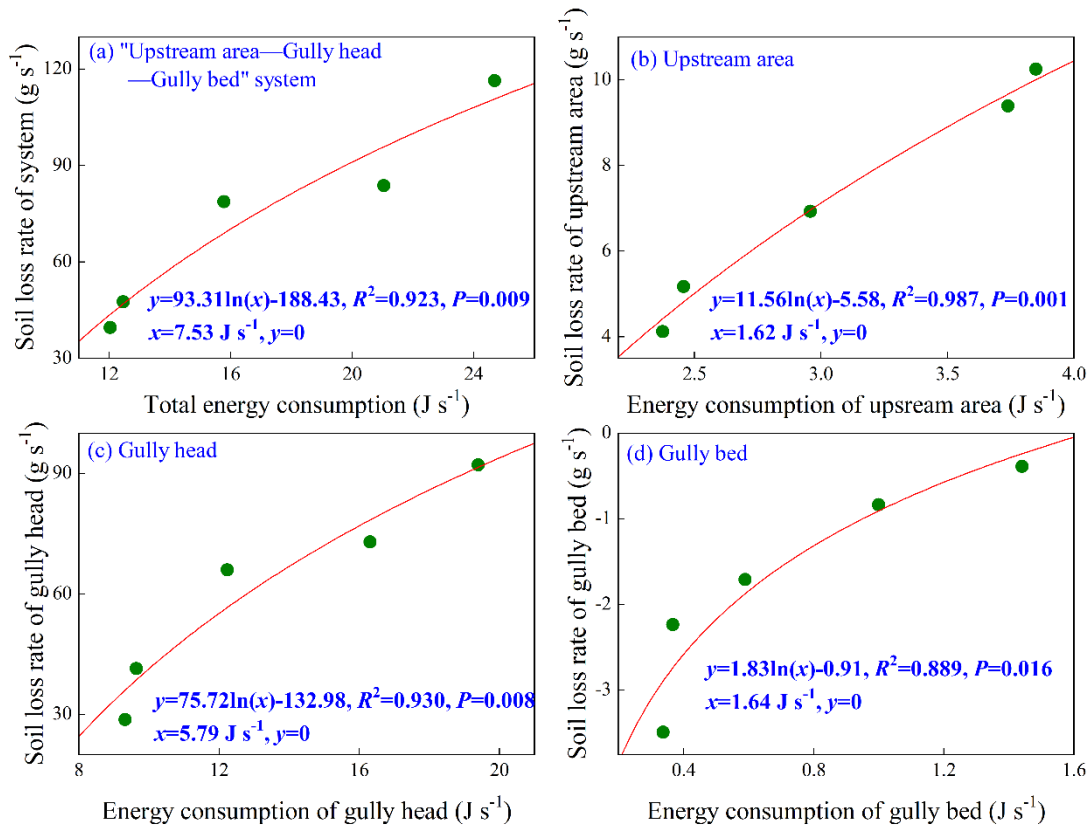


Figure 14 Relationships between soil loss rate of “upstream area-gully head-gully bed” system and three individual landform units and runoff energy consumption

4 Discussion

4.1 Spatial-temporal changes in hydraulic properties

This study ~~revealed~~ showed that the runoff velocity at the headcut brink-point (V_b) firstly raised and then gradually stabilized with ~~time~~ experimental duration (Fig. 5a4a), which was closely corresponded to the gradually decreased runoff width on the upstream area ~~with~~ over time (Shi et al., 2020a). However, this result was inconsistent with Zhang et al (2016, 2018) and Shi et al (2020b) who reported that the V_b decreased over time, which was mainly due to the gradually increased roughness and resistance of underlying surface over time reducing the runoff velocity ~~in their studies~~ (Battany and Grismer, 2015; Su et al., 2015). The further analysis of power function between V_b and time ($V_b=a \cdot t^b$, Table 1) showed that the a -value increased but the b -value showed a weak variation with the inflow discharge increased, indicating that upstream flow ~~discharge~~ can improve initial V_b but not affect its change trend over time. ~~Therefore, we can extrapolate the erosion process and rule~~

581 of upstream area from this simulation test to the actual ground situation. By contrast, the jet velocity
582 entry to plunge pool (V_e) and jet shear stress (τ_j) experienced a gradually decreased process (Fig.
583 ~~5e4c, 5e4e~~), which was mainly attributed to the fact that shortening of jet flow height caused by the
584 development of several second-headcut steps caused more energy consumption in plunge
585 pools and the lower potential energy at headcut brink-point due to the shortened jet flow height
586 upstream flow undercutting headcut brink point (Guo et al., 2019; Jiang et al., 2020). This result,
587 however, differed from the finding of Zhang et al. (2016) who stated the V_e and τ_j remained stable as
588 the experiments progressed, which was mainly attributed to the weak change of jet-flow height
589 induced by slow headcut retreat. This comparison manifested that the jet flow properties was
590 strongly determined by the headcut retreat process.

591 For the runoff hydraulic of upstream area (UA) and gully bed (GB), the Reynold number Re of
592 UA and GB initially increased and gradually stabilized, but the Froude number Fr showed an
593 opposite trend. This phenomenon was agreed with previous studies (e.g. Su et al., 2015; Zhang et al.,
594 2016; Shi et al., 2020a). Besides, ~~for the same upstream inflow discharge,~~ the Re and Fr of UA were
595 larger than that of GB by 50.5%-65.9% and 1.39-2.04 times, respectively, under same inflow
596 discharge upstream gully head, indicating that the runoff turbulence became weaker after the runoff
597 of UA passed the gully head and experienced plunge pool erosion (Shi et al., 2020a). More evidently,
598 the runoff on UA was in the supercritical-transition and supercritical-turbulent flow regime ($Re > 500$,
599 $Fr > 1$), whereas the runoff on GB belonged to subcritical-transition and subcritical-turbulent flow
600 regime ($Re > 500$, $Fr < 1$). However, Su et al. (2015) found that the steady state Re of gully bed was
601 higher than that of upstream area, which was mainly attributed to the difference in slope gradient. In
602 their study, The above result was supported by Shi et al. (2020a) who stated that the Re of gully bed
603 decreased by 1.5% - 30% as the flow fell from the upstream area, but Su et al. (2015) suggested that
604 the steady state Re of gully bed was higher than that of upstream area. In the study of Su et al. (2015),
605 the larger gully bed slope gradient than upstream area would accelerate the runoff velocity and thus
606 enhance flow turbulence (Bennett, 1999; Pan et al., 2016). Furthermore, Our study found that
607 temporal variation in the shear stress (τ) and stream power (ω) of UA was similar with GB, and,
608 compared to UA, the τ and ω of GB increased and decreased by 2.8% - 15.7% and 49.2% - 65.9%,

609 respectively. The increased shear stress was caused by the decrease of flow velocity on gully bed,
610 and the drastically decreased stream power can reflect the energy consumption of flow for
611 transporting sediment on gully bed. This result was different from some previous experimental
612 studies on gully and bank gully. ~~For example, the result from the study of Shi et al. (2020a) indicated~~
613 ~~that the τ of gully bed decreased by 65.9%–67.1%, compared to catchment area, and a similar result~~
614 ~~was also found during bank gully headcut erosion (Su et al., 2015) under different conditions.~~
615 Previous studies ~~also~~ have proven that the lots of factors including plunge pool size, slope gradient,
616 initial step height, and soil texture influenced change in the hydraulic properties from upstream area
617 to gully bed is affected by various factors ~~including plunge pool size, slope gradient, initial step~~
618 ~~height, and soil texture~~ (Bennett and Casali, 2001; Wells et al., 2009a, 2009b).

619 **4.2 Spatial-temporal change in runoff energy consumption and soil erosion**

620 Our study revealed that the accumulated runoff energy consumption of the upstream area (UA),
621 gully headcut (GH) and gully bed (GB) linearly increased over time (Fig. 98), indicating the
622 spatial-temporal change in energy consumption maintained a relatively steady state during gully
623 headcut erosion. However, the flow energy consumption of bank gully in three landform units
624 logarithmically increased over time (Su et al., 2015). This difference further manifested that the
625 runoff energy consumption of different landform units depends on gully type to some extent as well
626 as soil texture, slope and headwall height (Wells et al., 2009a). Besides, under this flow discharge
627 conditions, the proportion of energy consumption to the total flow energy ranged from 91.12% to
628 99.90%, indicating that almost all of flow energy was consumed during headcut erosion.
629 Furthermore, the proportion of energy consumption in UA, GH and GB was 15.6%-19.8%,
630 77.3%-78.6% and 2.8%-5.8%, respectively (Fig. 109), which was also indirectly supported by the
631 study of Su et al. (2015) who suggested that the runoff energy consumption per unit soil loss from
632 upstream area, headcut and gully bed is 17.4%, 70.5% and 12.0%, respectively. This further signified
633 that the gully head consumed the most of runoff energy (77.5% on average) during headcut
634 migration. The flow energy must be consumed to surmount the soil resistance as headcut migrates,
635 and the consumed energy was mainly focused on headwall and plunge pool development (Alonso et
636 al., 2002).

637 In terms of soil loss, our study indicated that the soil loss rate of the “UA-GH-GB” system
638 initially increased to the peak value and then gradually declined and stabilized (Fig. 410), which
639 was consistent with the results of many studies on rill and gully headcut erosion under different
640 conditions (slope, initial step height, flow discharge, soil type, soil stratification) (Bennett, 1999;
641 Bennett and Casalí, 2001; Gordon et al., 2007; Wells et al., 2009a; Shi et al., 2020a). Both the scour
642 depth and sediment production increased in the initial period of underlying surface adjustment, while
643 once the plunge pool development was maintained, and sediment yield decreased and gradually
644 stabilized (Bennett et al., 2000). In addition, the significant difference in soil loss process was found
645 among the three landform units. The soil loss of UA and GH decreased logarithmically over time,
646 which was similar with several studies (e.g., Su et al., 2015; Shi et al., 2020b). Nevertheless, the GB
647 was always characterized by sediment deposition for the inflow discharge of $< 4.8 \text{ m}^3 \text{ h}^{-1}$, whereas
648 the sediment was deposited firstly and then gradually transported as the inflow discharge increased to
649 6.0 and $7.2 \text{ m}^3 \text{ h}^{-1}$. Similar ~~results~~phenomena were also found in some previous studies on rill
650 heacut erosion (Bennett, 1999; Bennett and Casalí, 2001; Gordon et al., 2007; Wells et al., 2009a).
651 This further indicated that soil loss/deposition process of gully system was significantly influenced
652 by three landform units, and especially, the most of flow energy (77.5%) consumed at gully heads
653 due to jet flow erosion strongly weakened sediment transport capacity of flow on gully bed and thus
654 changed the soil loss/deposition process of gully system. However, Su et al. (2014, 2015) revealed a
655 larger soil loss volume or soil loss rate in gully bed than upstream area and headwall during bank
656 gully headcut erosion. This difference between our study and Su et al. (2014, 2015) is primarily
657 caused by the difference in slope gradient. The gully bed slope (20°) of bank gully was larger than
658 that (3°) of our study, indicating the runoff on gully bed of bank gully had stronger sediment
659 transport capacity (Zhang et al., 2009; Ali et al., 2013; Wu et al., 2016, 2018). Besides, some previous
660 also proved that the soil type, surface roughness, slope-length, groundwater/surface runoff were the
661 main factors influencing soil loss by gully erosion (Amare et al., 2020; Li et al., 2021). In view of the
662 proportion of soil loss, the proportion of UA and GH was 9.5% - 11.4% and 88.6% - 90.5%,
663 respectively, of which the proportion of deposited sediment on GB to the sediment yield from UA
664 and GH can reach up to 0.4% - 10.3%. This result fully demonstrated that the gully head is the main

665 source of sediment production during gully headcut erosion (Oostwoud-Wijdenes & Bryan, 1994;
666 Zhao, 1994; Su et al., 2014), and also manifested the necessary and importance of gully headcut
667 erosion controlling in gully-dominated region ([Amare et al., 2019](#)).

668 **4.3 Hydrodynamic characteristics of headcut erosion**

669 The significantly different relationships between soil loss and jet or hydraulic characteristics
670 ~~was~~ were found among UA, GH, and GB. The soil loss rate of UA exponentially increased with five
671 hydraulic parameters (runoff velocity, Reynold number, Froude number, runoff shear stress and
672 stream power), indicating that soil loss of UA showed a stronger sensitive response to increasing
673 hydraulic properties. This could attribute to the frequent bank collapse on UA accelerating soil loss
674 (Wells et al., 2013; Qin et al., 2018). However, the sediment deposition rate of GB linearly decreased
675 with the five hydraulic parameters, signifying that sediment deposition on GB decreased at a stable
676 state with the increase of hydraulic parameters. Therefore, the sediment deposition rate would reach
677 zero when the five hydraulic parameters increased to the critical values, implying that the
678 transformation of sediment deposition to sediment transport on GB would be triggered. Furthermore,
679 the shear stress is the optimal parameter describing soil loss process of UA and GB, which differed
680 from some studies on hillslope/[gully](#) erosion hydrodynamic characteristics (Zhang et al., 2009; Shen
681 et al., 2019; Ma et al., 2020; [Sidorchuk, 2020](#)). Most of studies have verified that stream power is the
682 superior hydrodynamic parameter describing soil detachment process. This comparison also fully
683 illustrated the great difference in hydrodynamic characteristic between hillslope erosion and headcut
684 erosion. In this study, the soil loss of gully head (including plunge pool erosion) was significantly
685 affected by jet properties. It's confirmed that the plunge pool erosion by jet flow becomes a crucial
686 process controlling gully head migration and sediment production (Oostwoud-Wijdenes et al., 2000).
687 Consequently, the plunge pool erosion theory is usually employed to build several headcut retreat
688 models (Alonso et al., 2002; Campo-Bescós et al., 2013). Although the weak correlation between soil
689 loss of gully head and flow velocity at headcut breakpoint, the larger flow velocity resulted from
690 increasing inflow discharge would improve the shear stress of jet flow impinging gully bed, and thus
691 the gully headcut suffered stronger incisional erosion of the plunge pool. However, in fact, the soil
692 loss of gully head was also affected by on-wall flow erosion (Chen et al., 2013; [Guo et al., 2021a](#)),

693 and thus more studies should be conducted to clear the effect of on-wall flow properties on [headcut](#)
694 [headwall](#) erosion.

695 From the energy consumption perspective, the soil loss rate of the three landform units
696 significantly and logarithmically increased with the energy consumption, and the similar change
697 trend was also found in the study of Su et al. (2015). This finding suggests that energy consumption
698 could be considered as the available parameter to estimate the soil loss of gully headcut erosion (Shi
699 et al., 2020b). Furthermore, we found the critical energy consumption initiating soil erosion of UA,
700 GH, and GB are 1.62 J s^{-1} , 5.79 J s^{-1} and 1.64 J s^{-1} , respectively, indicating the soil loss of gully head
701 (including plunge pool) needs more flow energy consumption (Zhang et al., 2018; Shi et al., 2020a,
702 2020b). This phenomenon can be attributed to the fact that the more runoff energy was consumed at
703 the gully headwall and plunge pool erosion than UA and GB and thus resulted in more severe soil
704 loss during headcut erosion. [In addition, we found that the critical energy consumption activating soil](#)
705 [loss of “UA-GH-GB” system was lower the sum of critical energy consumption initiating soil loss](#)
706 [and sediment transport of three landform units \(\$9.05 \text{ J s}^{-1}\$ \). This result was closely related to mass](#)
707 [failures such as gully head and gully bank collapse can contribute the additional energy into the flow.](#)
708 [So, the role of gravitational erosion in controlling gully erosion process should be clarified in the](#)
709 [future studies.](#)

710 **[5 Implication, significance and limitations of this study](#)**

711 [Gully erosion has been studied for nearly a century, but its process and dynamic mechanism are](#)
712 [still difficult to clearly understand and reveal. Given this, our study attempted to clarify the](#)
713 [spatial-temporal changes in flow hydraulic characteristics, energy consumption and soil loss and](#)
714 [expound the response of soil loss to runoff properties and energy consumption during headcut](#)
715 [erosion through a series of simulation experiment under controlled conditions. These results could be](#)
716 [extended to wider conditions, such as gully scale, flow discharge determined by rainfall and drainage](#)
717 [area, which can promote the understanding of process and mechanism of gully erosion under real](#)
718 [ground conditions as well as the modelling and prediction of gully erosion. Especially, the variation](#)
719 [and proportion of energy consumption along “UA-GH-GB” in the process of gully erosion and its](#)
720 [influence on sediment yield were clearly elucidated in this study, which has an important guiding](#)

721 significance for gully erosion control practice and restoration efforts. We can design some
722 engineering and/or vegetation measures at gully heads to pre-consume the most flow energy and the
723 energy dissipation structures could be designed and installed at the position where plunge pool
724 develops. Also, the appropriate size of these measures also can be determined to ensure the flow
725 energy of different landform units was lower than the corresponding critical energy consumption.

726 However, there are some potential limitations in our study. First, considering the complex
727 effects of lots of factors on gully erosion, the flow discharge ~~upstream gully heads~~ was designed as
728 the core factors affecting gully erosion in our study, and ~~the five levels of flow discharge~~~~the two~~
729 ~~factors~~ was generated according to the rainfall, landform and gully morphology. But it is not really
730 same as the actual ground situations, such as the flow discharge upstream gully heads would not be
731 constant during a rainfall event. Second, it has not been confirmed how well our experimental results
732 are in line with the actual ground results. Therefore, further studies need to verify the experimental
733 results with the actual situations, so that the study results can be practiced and applied under actual
734 rainfall conditions. Third, in the future research, gully erosion experiments under different control
735 measures should be carried out to identify suitable gully erosion prevention measures. Although the
736 earlier-noted imperfection represents the limitation of our study, we still clearly demonstrated the
737 temporal-spatial change in hydraulic properties and soil loss during headcut erosion and quantify the
738 response relationships of soil loss of different landform units to energy consumption, which is of
739 great significance for deepening the understanding of the gully process and hydrodynamic
740 mechanism. Also, our results can provide valuable ideas and scientific basis for the construction of
741 gully erosion model and the design of gully erosion prevention measures.

743 **Summary**

744 This study investigated the temporal-spatial changes in flow hydraulic, energy consumption and
745 soil loss during headcut erosion based on a series of scouring experiments of gully headcut erosion.
746 The jet properties of gully head (GH) were significantly affected by upstream inflow discharge. The
747 upstream area (UA) and gully bed (GB) had similar temporal changes in Reynold number, Froude
748 number, shear stress and stream power. The flow was supercritical on UA, but subcritical on GB, and

749 the turbulent degree was enhanced by the increasing inflow discharge. The flow Reynold number,
750 shear stress and stream power decreased by 56.0%, 63.8% and 55.9%, respectively, but Froude
751 number increased by 7.9% when flow passed the gully headcut and plunge pool. The accumulated
752 energy consumption at UA, GH and GB linearly increased with time. Overall, 91.12% - 99.90% of
753 total flow energy was consumed during headcut erosion, of which the GH accounted foreonsumed
754 77.5% of the total runoff energy dissipation followed by UA (18.3%) and GB (4.0%). The soil loss of
755 UA and GH decreased logarithmically over time, whereas the GB was mainly characterized by
756 sediment deposition. The GH ~~ean~~ and UA contributed 88.5% and 11.5% of total soil loss,
757 respectively, of which 3.8% sediment production was deposited on GB. The soil loss of UA and GH
758 and the sediment deposition of GB were significantly affected by hydraulic and jet properties. Our
759 study revealed that the critical energy consumption to initiate soil erosion of UA, GH and GB are
760 1.62 J s^{-1} , 5.79 J s^{-1} and 1.64 J s^{-1} , respectively. The runoff energy consumption could be considered
761 as a non-negligible parameter to predict ~~soil loss of~~ gully headcut erosion.

762 **Data availability**

763 At present, the original data are not publicly accessible because of a situation that we don't have
764 permission to share data according to the requirement of the funded program and our institute.
765 However, we are pleasure to share all data plotted in figures in this study for other colleagues.

766 **Author contribution**

767 Mingming Guo and Wenlong Wang designed the experiments. Mingming Guo, Zhuoxin Chen,
768 Tianchao Wang, Qianhua Shi, Man Zhao and Lanqian Feng carried out the experiments. Zhuoxin
769 Chen produced and processed the digital elevation model of erosion landform. Mingming Guo and
770 Wennlong Wang written and prepared the manuscript with contributions from all co-authors.

771 **Competing interests:**

772 The authors declare that they have no conflict of interest.

773 Acknowledgments

774 This work was supported by the National Natural Science Foundation of China ([42077079](#),
775 [41571275](#))-~~and~~, [the China Postdoctoral Science Foundation \(2020M681062\)](#), and the National Key
776 Research and Development Program of China (2016YFC0501604). Acknowledgement for the data
777 support from "Loess Plateau Data Center, National Earth System Science Data Sharing Infrastructure,
778 National Science & Technology Infrastructure of China. (<http://loess.geodata.cn>)".

779 References

- 780 Addisie, M.B., Ayele, G.K., Gessess, A.A., Tilahun, S.A., Zegeye, A.D., Moges, M.M., ... Steenhuis, T.S.:
781 Gully head retreat in the sub-humid Ethiopian Highlands: The Ene-Chilala catchment, *Land Degradation &*
782 *Development*, 28, 1579–1588, <https://doi.org/10.1002/ldr.2688>, 2017.
- 783 Ali, M., Seeger, M., Sterk, G., Moore, D.: A unit stream power based sediment transport function for overland
784 flow. *Catena*. 101, 197-204. <https://doi.org/10.1016/j.catena.2012.09.006>
- 785 Alonso, C.V., Bennett, S.J., Stein, O.R., 2002. Predicting head cut erosion and migration in concentrated flows
786 typical of upland areas, *Water Resources Research*, 38, 39-1–39-15, <http://dx.doi.org/10.1029/2001WR001173>,
787 2013.
- 788 [Amare, S., Keesstra, S., van der Ploeg, M., Langendoen, E., Steenhuis, T., Tilahun, S.: Causes and controlling](#)
789 [factors of Valley bottom Gullies. *Land*, 8\(9\), 141, <https://doi.org/10.3390/land8090141>, 2019.](#)
- 790 [Amare, S., Langendoen, E., Keesstra, S., Ploeg, M. V. D., Gelagay, H., Lemma, H., van der Zee, S. E.:](#)
791 [Susceptibility to Gully Erosion: Applying Random Forest \(RF\) and Frequency Ratio \(FR\) Approaches to a](#)
792 [Small Catchment in Ethiopia. *Water*, 13\(2\), 216, <https://doi.org/10.3390/w13020216>, 2021.](#)
- 793 [Arabameri, A., Chen, W., Lombardo, L., Blaschke, T., Tien Bui, D.: Hybrid computational intelligence models](#)
794 [for improvement gully erosion assessment. *Remote Sensing*, 12\(12\), <https://doi.org/10.3390/rs12010140>, 140,](#)
795 [2020.](#)
- 796 [Battany, M.C., Grismer, M.E.: Rainfall runoff and erosion in Napa Valley vineyards: effects of slope, cover](#)
797 [and surface roughness, *Hydrological Processes*, 14\(7\), 1289-1304,](#)
798 [https://doi.org/10.1002/\(SICI\)1099-1085\(200005\)14:7<1289::AID-HYP43>3.0.CO;2-R](https://doi.org/10.1002/(SICI)1099-1085(200005)14:7<1289::AID-HYP43>3.0.CO;2-R), 2015.
- 799 Beer, C.E., Johnson, H.P.: Factors in gully growth in the deep loess area of western Iowa. *Transactions of*
800 *ASAE*, 6, 237–240, <https://doi.org/10.13031/2013.40877>, 1963.
- 801 [Belayneh, M., Yirgu, T., Tsegaye, D.: Current extent, temporal trends, and rates of gully erosion in the Gumara](#)
802 [watershed, northwestern Ethiopia, *Global Ecology and Conservation*, 24, e01255,](#)
803 <https://doi.org/10.1016/j.gecco.2020.e01255>, 2020.
- 804 Bennett, S.J., Casali, J.: Effect of initial step height on headcut development in upland concentrated flows.
805 *Water Resources Research*, 37, 1475–1484, <https://doi.org/10.1029/2000WR900373>, 2001.
- 806 Bennett, S.J.: Effect of slope on the growth and migration of headcuts in rills, *Geomorphology*, 30, 273–290,
807 [https://doi.org/10.1016/S0169-555X\(99\)00035-5](https://doi.org/10.1016/S0169-555X(99)00035-5), 1999.
- 808 Bennett, S.J., Alonso, C.V.: Turbulent flow and bed pressure within headcut scour holes due to plane
809 reattached jets, *Journal of Hydraulic Research*, 44, 510–521, <https://doi.org/10.1080/00221686.2006.9521702>,
810 2006.

811 Bennett, S.J., Alonso, C.V., Prasad, S.N., Romkens, M.J.: Experiments on headcut growth and migration in
812 concentrated flows typical of upland areas, *Water Resources Research*, 36, 1911–1922,
813 <https://doi.org/10.1029/2000WR900067>, 2000.

814 [Bogale, A. G., Aynalem, D. W., Adem, A. A., Mekuria, W., Tilahun, S.: Spatial and temporal variability of soil](#)
815 [loss in gully erosion in upper Blue Nile basin, Ethiopia, *Applied Water Science*, 10\(5\), 106,](#)
816 <https://doi.org/10.1007/s13201-020-01193-4>, 2020.

817 Campo-Bescós, M.A., Flores-Cervantes, J.H., Bras, R.L., Casalí, J., Giráldez, J.V.: Evaluation of a gully
818 headcut retreat model using multitemporal aerial photographs and digital elevation models, *Journal of*
819 *Geophysical Research: Earth Surface*, 118, 2159–2173, <https://doi.org/10.1002/jgrf.20147>, 2013.

820 Chaplot, V., Giboire, G., Marchand, P., Valentin, C.: Dynamic modelling for linear erosion initiation and
821 development under climate and land-use changes in northern Laos, *Catena*, 63, 318–328,
822 <https://doi.org/10.1016/j.catena.2005.06.008>, 2005.

823 Che, X.L.: Study of distribution characteristic and evolution of headward erosion on Dongzhi tableland of the
824 loess gully region, Yangling: Northwest A&F University, pp. 66-67, (In Chinese), 2012.

825 Chen, A., Zhang, D., Peng, H., Fan, J., Xiong, D., Liu, G.: Experimental study on the development of collapse
826 of overhanging layers of gully in Yuanmou Valley, China, *Catena*, 109, 177-185,
827 <https://doi.org/10.1016/j.catena.2013.04.002>, 2013.

828 De Baets, S., Poesen, J., Knapen, A., Galindo, P.: Impact of root architecture on the erosion-reducing potential
829 of roots during concentrated flow, *Earth Surface Processes and Landforms*, 32, 1323–1345,
830 <https://doi.org/10.1002/esp.1470>, 2007.

831 de Vente, J., Poesen, J.: Predicting soil erosion and sediment yield at the basin scale: Scale issues and
832 semi-quantitative models, *Earth-Science Reviews*, 71, 95–125, <https://doi.org/10.1016/j.earscirev.2005.02.002>,
833 2005.

834 DeLong, S.B., Johnson, J., Whipple, K.: Arroyo channel head evolution in a flash-flood-dominated
835 discontinuous ephemeral stream system, *Geological Society of America Bulletin*, 126, 1683–1701,
836 <https://doi.org/10.1130/B31064.1>, 2014.

837 Descroix, L., González Barrios, J.L., Viramontes, D., Poulenard, J., Anaya, E., Esteves, M., Estrada, J.: Gully
838 and sheet erosion on subtropical mountain slopes: their respective roles and the scale effect, *Catena*, 72, 325–
839 339, <https://doi.org/10.1016/j.catena.2007.07.003>, 2008.

840 Dotterweich, M., Rodzik, J., Zglobicki, W., Schmitt, A., Schmidtchen, G., Bork, H.R.: High resolution gully
841 erosion and sedimentation processes, and land use changes since the Bronze Age and future trajectories in the
842 Kazimierz Dolny area (Nałęczów Plateau, SE-Poland), *Catena*, 95, 50–62,
843 <https://doi.org/10.1016/j.catena.2012.03.001>, 2012.

844 Flores-Cervantes, J., Istanbuluoglu, E., Bras, R.: Development of gullies on the landscape: A model of
845 headcut retreat resuUAing from plunge pool erosion, *Journal of Geophysical Research*, 111, 1–14,
846 <https://doi.org/10.1029/2004JF000226>, 2006.

847 Frankl, A., Stal, C., Abraha, A., Nyssen, J., Rieke-Zapp, D., DeWulf, A., Poesen, J.: Detailed recording of
848 gully morphology in 3D through image-based modelling, *Catena*, 127, 92–101,
849 <https://doi.org/10.1016/j.catena.2014.12.016>, 2015.

850 Fu, B.J., Liu, Y., Lv, Y.H., He, C.S., Zeng, Y., Wu, B.F.: Assessing the soil erosion control service of
851 ecosystems change in the Loess Plateau of China, *Ecological Complexity*, 8, 284-293,
852 <https://doi.org/10.1016/j.ecocom.2011.07.003>, 2011.

853 Gordon, L.M., Bennett, S.J., Wells, R.R., Alonso, C.V.: Effect of soil stratification on the development and
854 migration of headcuts in upland concentrated flows, *Water Resources Research*, 43, W07412,
855 <https://doi.org/10.1029/2006WR005659>, 2007.

856 Guo, M., Wang, W., Shi, Q., Chen, T., Kang, H., Li, J.: An experimental study on the effects of grass root
857 density on gully headcut erosion in the gully region of China's Loess Plateau, *Land Degradation &
858 Development*, 30, 2107–2125, <https://doi.org/10.1002/ldr.3404>, 2019.

859 Guo, M., Wang, W., Wang, T., Wang, W., Kang, H.: Impacts of different vegetation restoration options on
860 gully head soil resistance and soil erosion in loess tablelands, *Earth Surface Processes and Landforms*, 45(4),
861 1038-1050, <https://doi.org/10.1002/esp.4798>, 2020a.

862 Guo, M.M., Wang, W.L., Kang, H.L., Yang, B.: Changes in soil properties and erodibility of gully heads
863 induced by vegetation restoration on the Loess Plateau, China, *Journal of Arid Land*, 10(5), 712-725,
864 <https://doi.org/10.1007/s40333-018-0121-z>, 2018.

865 Guo, M.M., Wang, W.L., Li, J.M., Bai, Y., Kang, H.L., Yang, B.: Runoff characteristics and soil erosion
866 dynamic processes on four typical engineered landforms of coalfields: An in-situ simulated rainfall
867 experimental study, *Geomorphology*, 349, 106896, <https://doi.org/10.1016/j.geomorph.2019.106896>, 2020b.

868 [Guo, M.M., Lou, Y.B., Chen, Z.X., Wang, W.L., Feng, L.Q., Zhang, X.Y.: The proportion of jet flow and
869 on-wall flow and its effects on soil loss and plunge pool morphology during gully headcut erosion, *Journal of
870 Hydrology*, 598, 126220, <https://doi.org/10.1016/j.jhydrol.2021.126220>, 2021a.](#)

871 [Guo, M.M., Chen, Z.X., Wang, W.L., Wang, T.C., Wang, W.X., Cui, Z.Q.: Revegetation induced change in
872 soil erodibility as influenced by slope situation on the Loess Plateau, *Science of the Total Environment*, 772,
873 145540, <https://doi.org/10.1016/j.scitotenv.2021.145540>, 2021b.](#)

874 Hager, W.H.: Hydraulics of plane free overfall, *Journal of Hydraulic Engineering*, 109, 1683–1697,
875 [https://doi.org/10.1061/\(ASCE\)0733-9429\(1983\)109:12\(1683\)-](https://doi.org/10.1061/(ASCE)0733-9429(1983)109:12(1683)-), 1983.

876 Hanson, G.J., Robinson, K.M., Cook, K.R.: Prediction of headcut migration using a deterministic approach,
877 *Transactions of the ASAE*, 44(4), 525-531, <https://doi.org/10.13031/2013.6112>, 2001.

878 Hosseinalizadeh, M., Kariminejad, N., Chen, W., Pourghasemi, H.R., Alinejad, M., Behbahani, A.M.,
879 Tiefenbacher, J.P.: Gully headcut susceptibility modeling using functional trees, naïve Bayes tree, and random
880 forest models, *Geoderma*, 342, 1-11, <https://doi.org/10.1016/j.geoderma.2019.01.050>, 2019.

881 Ionita, I.: Gully development in the Moldavian Plateau of Romania, *Catena*, 68, 133–140,
882 <https://doi.org/10.1016/j.catena.2006.04.008>, 2006.

883 Ionita, I., Niacsu, L., Petrovici, G., Blebea-Apostu, A.M.: Gully development in eastern Romania: a case study
884 from Falciu Hills, *Natural Hazards*, 79, 113–138, <https://doi.org/10.1007/s11069-015-1732-8>, 2015.

885 [Jiang, Y., Shi, H., Wen, Z., Guo, M., Zhao, J., Cao, X., Fan, Y., Zheng, C.: The dynamic process of slope rill
886 erosion analyzed with a digital close range photogrammetry observation system under laboratory conditions,
887 *Geomorphology*, 350,106893, <https://doi.org/10.1016/j.geomorph.2019.106893>, 2020.](#)

888 Jiao, J.Y., Wang, W.Z., Hao, X.P.: Precipitation and erosion characteristics of rainstorm in different pattern on
889 Loess Plateau, *Journal of Arid Land Resources and Environment*, 13(1), 34-42, (In Chinese), 1999.

890 Kirkby, M.J., Bull, L.J., Poesen, J., Nachtergaele, J., Vandekerckhove, L.: Observed and modelled
891 distributions of channel and gully heads—with examples from SE Spain and Belgium, *Catena*, 50, 415–434,
892 [https://doi.org/10.1016/S0341-8162\(02\)00128-5](https://doi.org/10.1016/S0341-8162(02)00128-5), 2003.

893 Li, Binbing., Huang, Lei., Feng, Lin., Li, Peng., Yao, Jingwei., Liu, Fangming., Li, Junli., Tang, Hui.: Gully
894 sidewall expansion process on loess hill slope erosion, *Journal of Basic Science and Engineering*, 24(6),
895 1147-1158. (In Chinese), 2016.

896 Li, H., Cruse, R.M., Liu, X.B., Zhang, X.Y.: Effects of topography and land use change on gully development
897 in typical Mollisol region of Northeast China, *Chinese Geographical Science*, 26, 779-788,
898 <https://doi.org/10.1007/s11769-016-0837-7>, 2016.

899 Li, M., Song, X.Y., Shen, B., Li, H.Y., Meng, C.X.: Influence of vegetation change on producing runoff and
900 sediment in gully region of Loess Plateau, *Journal of Northwest Sci-Tech University of AgricuUAure and
901 Forestry (Natural Science Edition)*, 34, 117-120, (In Chinese), 2006.

902 [Li, Y., Mo, Y. Q., Are, K. S., Huang, Z., Guo, H., Tang, C., Abegunrin, T.P., Qin, Z.H, Kang, Z.W., Wang, X.:
903 Sugarcane planting patterns control ephemeral gully erosion and associated nutrient losses: Evidence from
904 hillslope observation. *Agriculture, Ecosystems & Environment*, 309, 107289,
905 <https://doi.org/10.1016/j.agee.2020.107289>, 2021.](#)

906 Li, Z., Zhang, Y., Zhu, Q., He, Y., Yao, W.: Assessment of bank gully development and vegetation coverage on
907 the Chinese Loess Plateau, *Geomorphology*, 228, 462–469, <https://doi.org/10.1016/j.geomorph.2014.10.005>,
908 2015.

909 Li, Z., Zheng, F.L., Liu, W.Z., Flanagan, D.C.: Spatial distribution and temporal trends of extreme temperature
910 and precipitation events on the Loess Plateau of China during 1961–2007, *Quaternary International*, 226(1-2),
911 92-100, <https://doi.org/10.1016/j.quaint.2010.03.003>, 2010.

912 Ma, Q., Zhang, K., Cao, Z., Wei, M., & Yang, Z.: Soil detachment by overland flow on steep cropland in the
913 subtropical region of China, *Hydrological Processes*, 34(8), 1810-1820, <https://doi.org/10.1002/hyp.13694>,
914 2020

915 Martínez-Casasnovas, J.A., Concepción Ramos, M., García-Hernández, David.: Effects of land - use
916 changes in vegetation cover and sidewall erosion in a gully head of the Penedès region (northeast Spain),
917 *Earth Surface Processes & Landforms*, 34, 1927-1937, <https://doi.org/10.1002/esp.1870>, 2009.

918 Nazari Samani, A., Ahmadi, H., Mohammadi, A., Ghoddousi, J., Salajegheh, A., Boggs, G., Pishyar, R.:
919 Factors Controlling Gully Advancement and Models Evaluation (Hableh Rood Basin, Iran), *Water Resources
920 Management*, 24, 1532–1549, <https://doi.org/10.1007/s11269-009-9512-4>, 2010.

921 Oostwoud-Wijdenes, D., Bryan, R.B.: The significance of gully headcuts as a source of sediment on low-angle
922 slopes at Baringo, Kenya, and initial control measures, *Advances in Geoecology*, 27, 205–231, 1994.

923 Oostwoud-Wijdenes, D., Poesen, J., Vandekerckhove, L., Ghesquiere, M.: Spatial distribution of gully head
924 activity and sediment supply along an ephemeral channel in a Mediterranean environment, *Catena*, 39, 147–
925 167, [http://202.194.143.28:80/rwt/SD/https/MSYXTLUQPJUB/10.1016/S0341-8162\(99\)00092-2](http://202.194.143.28:80/rwt/SD/https/MSYXTLUQPJUB/10.1016/S0341-8162(99)00092-2), 2000.

926 Pan, C., Ma, L., Wainwright, J., Shangguan, Z.: Overland flow resistances on varying slope gradients and
927 partitioning on grassed slopes under simulated rainfall, *Water Resources Research*, 52, 2490–2512,
928 <https://doi.org/10.1002/2015WR018035>, 2016.

929 Poesen, J., Nachtergaele, J., Verstraeten, G., Valentin, C.: Gully erosion and environmental change:
930 Importance and research needs, *Catena*, 50, 91-133, [https://doi.org/10.1016/S0341-8162\(02\)00143-1](https://doi.org/10.1016/S0341-8162(02)00143-1), 2003.

931 Qin, Chao., Zheng, Fenli., Wells Robert, R., Xu, Ximeng, Wang, Bin., Zhong, Keyuan.: A laboratory study of
932 channel sidewall expansion in upland concentrated flows, *Soil and Tillage Research*, 178, 22-31,
933 <https://doi.org/10.1016/j.still.2017.12.008>, 2018.

934 Reuter, H.I., Nelson, A., Jarvis, A.: An evaluation of void filling interpolation methods for SRTM data,
935 International Journal of Geographic Information Science, 21(9), 983-1008, 2007.

936 Rieke-Zapp, D.H., Nichols, M.H.: Headcut retreat in a semiarid watershed in the southwestern United States
937 since 1935, Catena, 87, 1–10, <https://doi.org/10.1016/j.catena.2011.04.002>, 2011.

938 Rodzik, J., Furtak, T., Zglobicki, W.: The impact of snowmelt and heavy rainfall runoff on erosion rates in a
939 gully system, Lublin Upland, Poland, Earth Surface Processes & Landforms, 34, 1938–1950,
940 <https://doi.org/10.1002/esp.1882>, 2009.

941 Rouse, H.: Engineering hydraulics. Hoboken, NJ: Wiley, 1950.

942 Sanchis, M.P., Torri, D., Borselli, L., Poesen, J.: Climate effects on soil erodibility, Earth Surface Processes &
943 Landforms, 33, 1082–1097, <https://doi.org/10.1002/esp.1604>, 2008.

944 Shen, N., Wang, Z., Zhang, Q., Chen, H., Wu, B.: Modelling soil detachment capacity by rill flow with
945 hydraulic variables on a simulated steep loessial hillslope, Hydrology Research, 50(1), 85-98,
946 <https://doi.org/10.2166/nh.2018.037>, 2018.

947 Shi, Q.H., Wang, W.L., Guo, M.M., Chen, Z.X., Feng, L.Q., Zhao, M., Xiao, H.: The impact of flow discharge
948 on the hydraulic characteristics of headcut erosion processes in the gully region of the Loess Plateau,
949 Hydrological processes, 34, 718-729, <https://doi.org/10.1002/hyp.13620>, 2020.

950 Shi, Q., Wang, W., Zhu, B., Guo, M.: Experimental study of hydraulic characteristics on headcut erosion and
951 erosional response in the tableland and gully regions of China, Soil Science Society of America Journal, 84,
952 700–716, <https://doi.org/10.1002/saj2.20068>, 2020.

953 [Sidorchuk, A.: The potential of gully erosion on the Yamal peninsula, West Siberia. Sustainability, 12\(1\), 260,
954 <https://doi.org/10.3390/su12010260>, 2020.](https://doi.org/10.3390/su12010260)

955 Stein, O., Julien, P., Alonso, C.: Mechanics of jet scour downstream of a headcut, Journal of Hydraulic
956 Research, 31, 723–738, <https://doi.org/10.1080/00221689309498814>, 1993.

957 Su, Z.A., Xiong, D.H., Dong, Y.F., Zhang, B.J., Zhang, S., Zheng, X.Y., Fang, H.D.: Hydraulic properties
958 of concentrated flow of a bank gully in the dry - hot valley region of southwest China, Earth Surface
959 Processes and Landforms, 40, 1351 - 1363. <https://doi.org/10.1002/esp.3724>, 2015.

960 Su, Z.A., Xiong, D.H., Dong, Y.F., Li, J.J., Yang, D., Zhang, J.H., He, G.X.: Simulated headward erosion of
961 bank gullies in the Dry-hot Valley Region of southwest China, Geomorphology, 204, 532–541,
962 <https://doi.org/10.1016/j.geomorph.2013.08.033>, 2014.

963 Sun, W.Y., Mu, X.M., Song, X.Y., Wu, D., Cheng, A.F., Qiu, B.: Changes in extreme temperature and
964 precipitation events in the Loess Plateau (China) during 1960–2013 under global warming, Atmospheric
965 Research, 168, 33-48, <https://doi.org/10.1016/j.atmosres.2015.09.001>, 2016.

966 Thompson, J.R.: Quantitative effect of watershed variables on rate of gully - head advancement. Transactions
967 of the ASABE, 7, 54 - 55, <https://doi.org/10.13031/2013.40694>, 1964.

968 Torri, D., Poesen, J.: A review of topographic threshold conditions for gully head development in different
969 environments, Earth-Science Reviews, 130, 73–85, <https://doi.org/10.1016/j.earscirev.2013.12.006>, 2014.

970 Valentin, C., Poesen, J., Li, Y.: Gully erosion: Impacts, factors and control, Catena, 63, 132–153,
971 <https://doi.org/10.1016/j.catena.2005.06.001>, 2005.

972 Vandekerckhove, L., Poesen, J., Govers, G.: Medium-term gully headcut retreat rates in southeast Spain
973 determined from aerial photographs and ground measurements, Catena, 50(2-4), 329-352,
974 [https://doi.org/10.1016/S0341-8162\(02\)00132-7](https://doi.org/10.1016/S0341-8162(02)00132-7), 2003.

975 Vandekerckhove, L., Poesen, J., Wijdenes, D.O., Nachtergaele, J., Tomás de Figueiredo.: Thresholds for gully
976 initiation and sedimentation in Mediterranean Europe, *Earth Surface Processes & Landforms*, 25(11),
977 1201-1220, [https://doi.org/10.1002/1096-9837\(200010\)25:11<1201::AID-ESP131>3.0.CO;2-L](https://doi.org/10.1002/1096-9837(200010)25:11<1201::AID-ESP131>3.0.CO;2-L), 2015.

978 Vanmaercke, M., Poesen, J., Mele, B.V., Demuzere, M., Bruynseels, A., Golosov, V., ... Yermolaev, O.: How
979 fast do gully headcuts retreat?, *Earth - Science Reviews*, 154, 336 - 355,
980 <https://doi.org/10.1016/j.earscirev.2016.01.009>, 2016.

981 Vannoppen, W., Vanmaercke, M., De Baets, S., Poesen, J.: A review of the mechanical effects of plant roots on
982 concentrated flow erosion rates, *Earth - Science Reviews*, 150, 666 - 678,
983 <https://doi.org/10.1016/j.earscirev.2015.08.011>, 2015.

984 Vanwalleghem, T., Bork, H.R., Poesen, J., Schmidtchen, G., Dotterweich, M., Nachtergaele, J., Bork, H.,
985 Deckers, J., Brüsck, B., Bungeneers, J., De Bie, M.: Rapid development and infilling of a buried gully under
986 cropland, Central Belgium, *Catena*, 63, 221–243, <https://doi.org/10.1016/j.catena.2005.06.005>, 2005.

987 Vanwalleghem, T., Van Den Eeckhaut, M., Poesen, J., Deckers, J., Nachtergaele, J., Van Oost, K., Slenters, C.:
988 Characteristics and controlling factors of old gullies under forest in a temperate humid climate: a case study
989 from the Meerdaal Forest (Central Belgium), *Geomorphology*, 56(1), 15–29,
990 [https://doi.org/10.1016/S0169-555X\(03\)00043-6](https://doi.org/10.1016/S0169-555X(03)00043-6), 2003.

991 Wells, R.R., Alonso, C.V., Bennett, S.J.: Morphodynamics of Headcut Development and Soil Erosion in
992 Upland Concentrated Flows, *Soil Science Society of America Journal*, 73, 521–530.
993 <https://doi.org/10.2136/sssaj2008.0007>, 2009a.

994 Wells, R.R., Bennett, S.J., Alonso, C.V.: Effect of soil texture, tailwater height, and pore - water pressure on
995 the morphodynamics of migrating headcuts in upland concentrated flows, *Earth Surface Processes and*
996 *Landforms*, 34, 1867 - 1877, <https://doi.org/10.1002/esp.1871>, 2009b.

997 Wells, R.R., Momm, H.G., Rigby, J.R., Bennett, S.J., Bingner, R.L., Dabney, S.M.: An empirical investigation
998 of gully widening rates in upland concentrated flows, *Catena*, 101, 114-121,
999 <https://doi.org/10.1016/j.catena.2012.10.004>, 2013.

1000 Wen, X., Wu, X., Gao, M.: Spatiotemporal variability of temperature and precipitation in Gansu province
1001 (northwest China) during 1951–2015, *Atmospheric Research*, 197, 132-149,
1002 <https://doi.org/10.1016/j.atmosres.2017.07.001>, 2017.

1003 [Wen, Y., Kasielke, T., Li, H., Zhang, B., Zepp, H.: May agricultural terraces induce gully erosion? a case study](https://doi.org/10.1016/j.scitotenv.2020.141715)
1004 [from the black soil region of northeast China. *Science of The Total Environment*, 750\(4\), 141715,](https://doi.org/10.1016/j.scitotenv.2020.141715)
1005 [https://doi.org/ 10.1016/j.scitotenv.2020.141715, 2020.](https://doi.org/10.1016/j.scitotenv.2020.141715)

1006 Wu, Bing., Wang, Zhanli., Zhang, Qingwei., Shen, Nan., Liu, June., Wang, Sha.: Evaluation of shear stress
1007 and unit stream power to determine the sediment transport capacity of loess materials on different slopes,
1008 *Journal of Soil & Sediments*, 18, 116–127, <https://doi.org/10.1007/s11368-017-1758-5>, 2018.

1009 Wu, B., Wang, Z., Shen, N., Wang, S.: Modelling sediment transport capacity of rill flow for loess sediments
1010 on steep slopes, *Catena*, 147, 453-462, <https://doi.org/10.1016/j.catena.2016.07.030>, 2016.

1011 Xia, L., Song, X.Y., Fu, N., Li, H.Y., Li, Y.L.: Impacts of land use change and climate variation on green water
1012 in the Loess Plateau Gully Region—A case study of Nanxiaohegou basin, *Journal of Hydraulic Engineering*,
1013 48(6), 678-688, (In Chinese), 2017.

1014 Xu, J.Z., Li, H., Liu, X.B., Hu, W., Yang, Q.N., Hao, Y.F., Zhen, H.C., Zhang, X.Y.: Gully Erosion Induced by
1015 Snowmelt in Northeast China: A Case Study, *Sustainability*, 11, <https://doi.org/10.3390/su11072088>, 2019.

1016 Xu, X.M., Zheng, F.L., Wilson, G.V., Wu, M.: Upslope inflow, hillslope gradient and rainfall intensity impacts
1017 on ephemeral gully erosion, *Land Degradation & Development*, 28, 2623-2635
1018 <https://doi.org/10.1002/ldr.2825>, 2017.

1019 Xu, X.M., Zheng, F.L., Qin, C., Wu, H.Y., Wilson, G.V.: Impact of cornstalk buffer strip on hillslope soil
1020 erosion and its hydrodynamic understanding, *Catena*, 149, 417-425,
1021 <https://doi.org/10.1016/j.catena.2016.10.016>, 2017.

1022 Xu, X.M., Wang, H.B., Zhao, J.Y., Liu, X.J.: Dynamic variation of soil erosion of Nanxiaohegou small
1023 watershed during 2004-2016, *Soil and Water Conservation in China*, 443(2), 59-61, (In Chinese), 2019.

1024 [Yang, C.T.: Potential energy and stream morphology, *Water Resource Research*, 7\(2\), 311-223,](https://doi.org/10.1029/WR007i002p00311)
1025 <https://doi.org/10.1029/WR007i002p00311>, 1971a.

1026 [Yang, C.T.: On river meanders, *Journal of Hydrology*, 13, 231-253,](https://doi.org/10.1016/0022-1694(71)90226-5)
1027 [https://doi.org/10.1016/0022-1694\(71\)90226-5](https://doi.org/10.1016/0022-1694(71)90226-5), 1971b.

1028 Zhang, B.J., Xiong, D.H., Su, Z.A., Yang, D., Dong, Y.F., Xiao, L., Zhang, S., Shi, L.T.: Effects of initial step
1029 height on the headcut erosion of bank gullies: a case study using a 3D photo-reconstruction method in the
1030 Dry-hot Valley region of southwest China, *Physical Geography*, 37, 409-429,
1031 <https://doi.org/10.1080/02723646.2016.1219939>, 2016.

1032 Zhang, B.J., Xiong, D.H., Zhang G.H., Zhang, S., Wu, H., Yang, D., Xiao, L., Dong, Y.F., Su, Z.A., Lu, X.N.:
1033 Impacts of headcut height on flow energy, sediment yield and surface landform during bank gully erosion
1034 processes in the Yuanmou Dry - hot Valley region, southwest China, *Earth Surface Processes & Landforms*,
1035 43(10), 2271-2282, <https://doi.org/10.1002/esp.4388>, 2018.

1036 Zhang, H.X.: The characteristics of hard rain and its distribution over the Loess Plateau, *Acta Geographica*
1037 *Sinica*, 38, 416-425, (In Chinese), 1983.

1038 Zhang, G.H., Liu, Y.M., Han, Y.F., Zhang, X.C.: Sediment transport and soil detachment on steep slopes: I.
1039 transport capacity estimation, *Soil Science Society of America Journal*, 73, 1291-1297,
1040 <https://doi.org/10.2136/sssaj2008.0145>, 2009.

1041 [Zhang, X., Fan, J., Liu, Q., Xiong D.: The contribution of gully erosion to total sediment production in a small](https://doi.org/10.1080/02723646.2017.1356114)
1042 [watershed in Southwest China, *Physical Geography*, 39\(3\), 1-18,](https://doi.org/10.1080/02723646.2017.1356114)
1043 <https://doi.org/10.1080/02723646.2017.1356114>, 2018.

1044 Zhao, A.C.: Analysis of control models of typical small watershed in gully area of Loess Plateau, the east part
1045 of Gansu Province, *Research of Soil and Water Conservation*, 1, 45-49, (In Chinese), 1994.

1046 Zhu, T.X.: Gully and tunnel erosion in the hilly Loess Plateau region, China, *Geomorphology*, 153, 144-155,
1047 <https://doi.org/10.1016/j.geomorph.2012.02.019>, 2012.